Acta Neuropathologica (2024) 147:32
https://doi.org/10.1007/s00401-023-02679-6

ORIGINAL PAPER

Transmembrane protein 97 is a potential synaptic amyloid beta receptor in human Alzheimer's disease

Martí Colom-Cadena[1] · Jamie Toombs[1] · Elizabeth Simzer[1] · Kristjan Holt[1] · Robert McGeachan[1] · Jane Tulloch[1] · Rosemary J. Jackson[1,2] · James H. Catterson[1] · Maxwell P. Spires-Jones[1] · Jamie Rose[1] · Lora Waybright[3] · Anthony O. Caggiano[3] · Declan King[1] · Francesco Gobbo[1] · Caitlin Davies[1] · Monique Hooley[1] · Sophie Dunnett[1] · Robert Tempelaar[1] · Soraya Meftah[1] · Makis Tzioras[1,3] · Mary E. Hamby[4] · Nicholas J. Izzo[4] · Susan M. Catalano[4] · Claire S. Durrant[1] · Colin Smith[5] · Owen Dando[1] · Tara L. Spires-Jones[1]

Received: 9 August 2023 / Revised: 24 December 2023 / Accepted: 24 December 2023

Abstract

Synapse loss correlates with cognitive decline in Alzheimer's disease, and soluble oligomeric amyloid beta (Aβ) is implicated in synaptic dysfunction and loss. An important knowledge gap is the lack of understanding of how Aβ leads to synapse degeneration. In particular, there has been difficulty in determining whether there is a synaptic receptor that binds Aβ and mediates toxicity. While many candidates have been observed in model systems, their relevance to human AD brain remains unknown. This is in part due to methodological limitations preventing visualization of Aβ binding at individual synapses. To overcome this limitation, we combined two high resolution microscopy techniques: array tomography and Förster resonance energy transfer (FRET) to image over 1 million individual synaptic terminals in temporal cortex from AD ($n=11$) and control cases ($n=9$). Within presynapses and post-synaptic densities, oligomeric Aβ generates a FRET signal with transmembrane protein 97. Further, Aβ generates a FRET signal with cellular prion protein, and post-synaptic density 95 within post synapses. Transmembrane protein 97 is also present in a higher proportion of post synapses in Alzheimer's brain compared to controls. We inhibited Aβ/transmembrane protein 97 interaction in a mouse model of amyloidopathy by treating with the allosteric modulator CT1812. CT1812 drug concentration correlated negatively with synaptic FRET signal between transmembrane protein 97 and Aβ. In human-induced pluripotent stem cell derived neurons, transmembrane protein 97 is present in synapses and colocalizes with Aβ when neurons are challenged with human Alzheimer's brain homogenate. Transcriptional changes are induced by Aβ including changes in genes involved in neurodegeneration and neuroinflammation. CT1812 treatment of these neurons caused changes in gene sets involved in synaptic function. These data support a role for transmembrane protein 97 in the synaptic binding of Aβ in human Alzheimer's disease brain where it may mediate synaptotoxicity.

Keywords Alzheimer's disease · Aβ · Synapses · TMEM97 · Sigma-2 · Cellular prion protein

✉ Tara L. Spires-Jones
Tara.spires-jones@ed.ac.uk

1 Centre for Discovery Brain Sciences and UK Dementia Research Institute, The University of Edinburgh, 1 George Square, Edinburgh EH8 9JZ, UK

2 Present Address: MassGeneral Institute for Neurodegenerative Diseases, Massachusetts General Hospital, Harvard Medical School, Boston, MA 02129, USA

3 Present Address: Scottish Brain Sciences, Edinburgh EH12 9DQ, UK

4 Cognition Therapeutics Inc., Pittsburgh, PA 15203, USA

5 Centre for Clinical Brain Sciences and Sudden Death Brain Bank, University of Edinburgh, Edinburgh EH16 4HB, UK

Abbreviations

Aβ	Amyloid beta
TMEM97	Transmembrane protein 97
PSD95	Postsynaptic density 95
PrPc	Cellular prion protein
PGRMC1	Progesterone receptor membrane component 1

Published online: 06 February 2024

Introduction

In Alzheimer's disease, synapse loss is an early event in the aetiology of the disease and is the strongest pathological correlate of cognitive decline [17, 56, 67]. The mechanism(s) underlying synapse degeneration, however, are still largely unknown [10]. We and others have observed that oligomeric amyloid beta (Aβ) peptide causes synaptic dysfunction, accumulates within in synapses, and is associated with synapse loss around plaques [34, 41, 52, 60, 64]. While it is clear that toxicity of tau and changes in non-neuronal cells are also important in disease pathogenesis [24], substantial evidence supports an important role for Aβ in synaptotoxicity early in the disease process in Alzheimer's [38]. As such, it is important to identify synaptic binding partners of Aβ which may mediate synaptotoxicity in human brain. Disrupting binding of Aβ with synaptic receptors is a promising therapeutic avenue as such interactions are "druggable", or able to be interrupted with standard pharmacological approaches [14].

Synaptic Aβ binding partners have been identified in cell culture systems and mouse models, but their human relevance is still debated (reviewed in [5, 30, 46, 63]). Among the Aβ binding candidates, cellular prion protein (PrP_c) represents the most studied, either alone or through a complex with mGluR5 [37, 62, 72, 79]. Other suggested Aβ binding partners at synapses include the α7-nicotinic receptor [49], Ephrin A4 [73], PSD95 [35, 50, 52] and LilrB2 [32]. An important outstanding question in the field is which of these potential partners binds Aβ in human synapses, as most binding partners have not been validated in Alzheimer's cases nor using human derived Aβ species [38, 63]. Further, in model systems, Aβ is often overexpressed or applied exogenously, and due to the "sticky" nature of Aβ oligomers, this can result in false positive signals for interacting partners, which has been highlighted as a problem for translation in the field [5].

TMEM97, transmembrane protein 97, is a promising potential synaptic binding partner of Aβ. TMEM97 was recently identified as the gene that codes for the Sigma-2 receptor [3]. Sigma-2 receptors have been studied for more than four decades and are drug targets for several conditions including cancer, pain and diverse CNS disorders [22, 58]; and most notably, a Sigma-2 modulator, CT1812, is in clinical development in Phase 2 trials for Alzheimer's disease and dementia with Lewy bodies [11, 21]. In the context of Alzheimer's, in 2014, Izzo and colleagues found that Sigma-2 modulators including CT1812 could displace Aβ synthetic oligomers from their synaptic receptors in cellular models and could improve cognitive deficits in a mouse model of Alzheimer's [27]. Yi et al.and Mondal et al.similarly found that Sigma-2 receptor ligands prevent neurodegeneration in a worm model expressing human amyloid precursor protein [44, 77].

Little is known about the pathophysiological role of Sigma-2, especially due to its unknown identity until the identification of TMEM97. TMEM97, initially known as MAC30 [47], is overexpressed in some cancers and it is believed to be a key player of cholesterol homeostasis [78] and calcium regulation [8, 74, 77]. Linking this function to Alzheimer's, in cellular models, TMEM97 has recently been shown to form a ternary complex with Progesterone receptor membrane component 1 (PGRMC1) and LDLR [55] that may control the internalization of monomers and oligomers of Aβ [54]. In addition, our group recently found increased levels of TMEM97 in synaptoneurosomes from Alzheimer's cases, compared to control, in a proteomics study [25], supporting a potential role in synaptotoxicity in humans.

Until the 2017 discovery that *TMEM97* encodes the Sigma-2 receptor [3], the understanding of the ability of Sigma-2 receptor modulators to displace Aβ oligomers from synapses was based off solely pharmacological/functional data, and data indicating that this effect was correlated with PGRCM1 expression. To date, there has been no direct interrogation of whether TMEM97, PGRMC1 and Aβ are found within the same synapses in human brain, whether CT1812 affects TMEM97 binding to Aβ within synapses, or whether PrPC binding to TMEM97 may underlie the ability of Sigma-2 receptor modulators to displace Aβ oligomers. The herein paper addresses these knowledge gaps for the first time.

The study of synapses in the human brain represents a technical challenge due to their small volumes, which are smaller than the diffraction limit of light microscopy, making colocalization studies difficult. In the present work we applied a new approach for the study of the close proximity of proteins in synapses in human post-mortem brain tissue. To visualize the potential interaction between Aβ and potential binding partners at synapses, we combined array tomography [43] and Föster resonance energy transfer (FRET) microscopy [20, 80]. Array tomography allows us to reach a 70nm axial resolution, which enables the identification of single synaptic terminals in three dimensions [31]. The combination of array tomography with FRET enhances the lateral resolution to ~ 10 nm in the selected single synaptic terminals allowing us to determine whether proteins are close enough to be interacting [23, 52].

The current study tests the hypothesis that TMEM97 interacts with Aβ in synapses in human Alzheimer's brain and that modulating this can recover synaptic phenotypes in model systems. We demonstrate that TMEM97 is a potential Aβ synaptic binding partner in human brain tissue and confirms that Sigma-2 receptor complex allosteric modulator CT1812 can reduce interactions between TMEM97 and Aβ in vivo. These findings shed light on the mechanisms

of action by which a Sigma-2 receptor modulator may be acting in the context of Alzheimer's, and may help further Alzheimer's therapeutic approaches, in both drug discovery and clinical development. Finally, this study enables further technical advances in the study of the still elusive synaptic structures involved in neurodegeneration.

Materials and methods

Human cases

Patients fulfilling clinical and neuropathological criteria for Alzheimer's disease ($n=11$ for array tomography, 6 for ELISA) [45], or cognitively healthy control cases ($n=9$ for array tomography, 6 for ELISA) were included in this study. Sample sizes were based on power calculations using effect size of 0.79 from our previous human array tomography studies looking at colocalization of clusterin and Aβ in synapses in Alzheimer's [29] indicating that $n=6$ per group is sufficient at power = 0.8 to detect a difference between colocalization of proteins at synapses between AD and controls (calculated using the WebPower package in R 4.1.2). A post-hoc power calculation using the results from the primary question in this study—whether Aβ and TMEM97 generate a FRET signal in human synapses—indicates that with our n and effect size, we have 100% power to detect a positive FRET signal (effect size 3.8 based on the % Aβ-TMEM97 FRET positive pixels within PSDs 38.4% ± 9.66 and the biological negative control—the % PSD-synaptophysin FRET positive pixels 1.75% ± 0.203). Clinical and neuropathological data were retrospectively obtained from the clinical charts available at the Edinburgh Brain Bank. Neuropathological stages were applied according to international recommendations [7, 45, 68]. Details of the human cases included are found in Table 1. Use of human tissue for post-mortem studies has been reviewed and approved by the Edinburgh Brain Bank ethics committee and the ACCORD medical research ethics committee, AMREC (ACCORD is the Academic and Clinical Central Office for Research and Development, a joint office of the University of Edinburgh and NHS Lothian, approval number 15-HV-016). The Edinburgh Brain Bank is a Medical Research Council funded facility with research ethics committee (REC) approval (16/ES/0084).

Mice

Mice expressing both human tau and the APP/PS1 transgene (APP/PS1 + Tau) were generated as previously described [51]. Briefly, two feeder lines were bred to produce experimental genotypes. The feeder lines were line 1: mice heterozygous for an APP/PS1 transgene and a CK-tTA driver transgene and homozygous for knockout of endogenous mouse tau; line 2: heterozygous for the Tg21221 human wild type tau transgene driven by CK-tTA and homozygous for knockout of endogenous mouse tau mouse tau [51]. APP/PS1 + Tau mice ($n=20$) and littermate control mice not expressing APP/PS1 nor tau ($n=20$) were aged to 9 months old before starting CT1812 treatment. Mice of both sexes were randomised into vehicle or control groups. Animal experiments were conducted in compliance with national and institutional guidelines including the Animals [Scientific Procedures Act] 1986 (UK), and the Council Directive 2010/63EU of the European Parliament and the Council of 22 September 2010 on the protection of animals used for scientific purposes, and had full Home Office ethical approval.

Mice were singly housed in a 12 h dark/light cycle with food and water ad libitum. Before dosing started, mice were habituated with double concentration Hartley's strawberry jelly 4 days during which time all mice learned to eat the entire serving of jelly within 5 min. CT1812 fumarate was dissolved in dimethyl sulfoxide (DMSO) and added to cold jelly solution to make up the final volume of 0.6 mg/ml concentration before being allowed to set. Each week, a batch of Hartley's strawberry jelly containing CT1812 or vehicle (plain triple strength jelly) was made. Mice were weighed at the beginning of each week to determine the weight of jelly to be given for that week, and were dosed daily for one month with jelly containing vehicle or CT1812 10 mg/kg/day (experimenters administering jelly were blind to condition). The jelly was delivered in a small petri dish on the floor of the home cage and mice were observed until all jelly was eaten to ensure the full dose was received following which the empty dish was removed.

After 28 days of treatment, mice were sacrificed by terminal anaesthesia. Blood was collected for drug levels then mice were perfused with phosphate-buffered saline (0.1 M) (PBS). Brains were removed and the cerebellum snap frozen for testing drug levels. One cerebral hemisphere (selected randomly) was drop fixed in 4% paraformaldehyde. The other hemisphere was dissected and entorhinal cortex processed for array tomography. The rest of the hemisphere was snap frozen for biochemical studies. Estimated percent receptor occupancy was calculated according to the formula (concentration/Ki)/[(concentration/Ki) + 1)], where Ki is determined by radioligand competition binding [27].

The main study combining array tomography and FRET experiments were performed on APP/PS1 + tau mice (n = 10) and control littermates ($n=8$). Details are found in Table S1. Standard array tomography imaging (without FRET) was performed on APP/PS1 + tau mice ($n=9$) and control littermates ($n=13$) to test whether there were any drug effects on synapse density.

Table 1 Demographic, clinical, neuropathological and genetic data of human cases

BBN	Case ID (Edinburgh)	Diagnosis (clinical)	*APOE* genotype	Brain weight (g)	Age (y)	Sex	PMI (h)	Braak NFT stage	Thal Aβ Phase	Study
001.28406	SD001/16	control	3/3	1437	79	m	72	II	2	FRET
001.28794	SD018/16	control	2/3	1289	79	f	72	I	0	FRET/ELISA
001.26495	SD024/15	control	3/3	1290	78	m	39	I	1	FRET/ELISA
001.28797	SD025/16	control	3/3	1301	79	m	57	0	0	FRET/ELISA
001.29086	SD034/16	control	3/3	1468	79	f	68	0	1	FRET/ELISA
BBN_19686	SD063/13	control	3/3	1320	77	f	75	I	1	FRET/ELISA
001.35181	SD003/19	control	3/4	1496	82	m	49	II	2	FRET
001.34131	SD029/18	control	3/4	1472	82	m	95	IV	3	FRET/ELISA
001.29082	SD031/16	control	3/4	1339	79	f	80	III	5	FRET
001.29695	SD004/17	Alzheimer's	3/4	1300	86	m	72	VI	5	FRET/ELISA
001.28771	SD010/16	Alzheimer's	3/3	1183	85	m	91	VI	5	FRET
001.32929	SD012/18	Alzheimer's	3/3	1354	85	f	80	VI	5	FRET
BBN_25739	SD014/15	Alzheimer's	3/4	1375	85	f	45	VI	5	FRET
001.35096	SD037/18	Alzheimer's	3/4	1209	72	m	103	VI	5	FRET
001.30973	SD039/17	Alzheimer's	3/4	1210	89	f	96	VI	5	FRET/ELISA
001.26718	SD040/15	Alzheimer's	3/4	1367	78	m	74	VI	5	FRET
BBN_24322	SD049/14	Alzheimer's	3/4	1410	80	m	101	VI	5	FRET
BBN_24527	SD056/14	Alzheimer's	3/3	1160	81	m	74	V	4	FRET
001.28410	SD005/16	Alzheimer's	3/3	NA	62	f	109	VI	5	FRET
001.29081	SD030/16	Alzheimer's	3/3	943	90	f	110	VI	5	FRET
001.29135	SD027/16	Alzheimer's	3/4	1275	90	m	73	VI	3	ELISA
001.30883	SD034/17	Alzheimer's	3/4	1060	61	f	69	VI	5	ELISA
001.30142	SD020/17	Alzheimer's	3/4	1054	88	f	112	VI	5	ELISA
001.29521	SD035/16	Alzheimer's	3/4	1221	95	m	96	VI	5	ELISA

BBN brain bank number, *NFT* neurofibrillary tangle, *NA* not available

Array tomography

Fresh brain tissue samples from human and mouse cases were collected and processed as previously described [31]. Briefly, small pieces of brain tissue comprising all cortical layers were fixed in 4% paraformaldehyde and 2.5% sucrose in 20mM PBS pH 7.4 for up to 3 h. Samples were then dehydrated through ascending concentrations of cold ethanol until embedding into LR White resin (Electron Microscopy Sciences, EMS), which was allowed to polymerize overnight at > 50 °C. Tissue blocks were then stored at room temperature until used. For each case, two blocks corresponding to BA20/21 for human cases, or one from entorhinal cortex for mouse samples, were cut into 70 nm thick sections using an ultramicrotome (Leica) equipped with a Jumbo Histo Diamond Knife (Diatome, Hatfield, PA). Ribbons of at least 20 consecutive sections were collected in gelatine subbed coverslips.

Seventy nm thick ribbons were immuno-labelled as described previously [31]. Briefly, coverslips were first incubated with Tris–glycine solution 5 min at room temperature followed by blocking of non-specific antigens with a cold-water fish blocking buffer (Sigma-Aldrich) for 30 min. Samples were then incubated for 2 h with primary antibodies, washed with Tris-buffered saline (TBS) solution and secondary antibodies applied for 30 min. After another TBS washing cycle, coverslips were mounted on microscope slides with Immu-Mount (Fisher Scientific) mounting media. For the detailed information of the primary and secondary antibodies used, please see Table S2.

Images of the same field of view of the consecutive sections were acquired using a Leica TCS8 confocal with 63 × 1.4 NA oil objective. In AD cases, images were acquired with a plaque in the field since our previous work demonstrated that synaptic Aβ accumulation is most prominent around plaques [29, 34]. Alexa fluor 488, Cy3 or Cy5 were sequentially excited with the 488, 552 or 638 laser lines and imaged in 500–550 nm, 570–634 nm or 649–710 nm spectral windows, respectively. For FRET analysis, the spectral window of the Cy5 (the acceptor, 649–710 nm) was also imaged under the excitation of Cy3 (the donor, 552 nm). This setting allowed us to record the transfer of energy from donor molecules to acceptors based on intensity (sensitized emission FRET, [23, 80], Fig. S1). Laser and detector settings were maintained through the whole study avoiding major saturation, which is only applied in figures for image visualization purposes.

Standard array tomography imaging (without FRET) was performed on APP/PS1 + tau mice ($n = 9$) and control littermates of mice ($n = 13$) to test whether there were any drug effects on synapse density. These images were acquired on a Ziess Axio Imager Z2 epifluorescence microscope with a 63 × 1.4 NA oil immersion objective and a CoolSNAP digital camera.

Images from consecutive sections were transformed into stacks using ImageJ [57, 59]. The following steps were performed using an in-house algorithm developed for array tomography image processing and analysis freely available (based on [13], available at https://github.com/Spires-Jones-Lab, Fig. S1). The consecutive images were first aligned using a rigid and affine registration. For the study of the immunoreactivity patterns, semi-automatic local threshold based on mean values was applied specifically for each channel yet common for all the included images. Importantly, only those objects detected in more than one consecutive Sect. (3D objects) were quantified, allowing us to reduce non-specific signals. The number of objects from each channel were quantified and neuropil concentration in mm^3 of tissue established after removing confounding structures (i.e. blood vessels or cell bodies). to investigate the relationship between channels, colocalization was based on a minimum overlap of 10% of the area of the synaptic terminals. Finally, in Alzheimer's cases, the effect of plaque proximity on concentration of objects in each channel or the colocalizing objects were also determined by calculating the Euclidean distance between the centroid of each object and the closest point to the plaque edge. The plaque edge was determined using a restrictive segmentation of the 6E10 channel to include only areas of contiguous staining (not including small Aβ positive puncta in the halo which we previously described [34]. Objects were then binned in 10 µm distances from the plaque edge.

For FRET analysis, donor-only (Cy3) and acceptor-only (Cy5) samples were imaged in each imaging session to calculate the donor-emission crosstalk with the acceptor emission (beta parameter) and the direct excitation of the acceptor by the donor excitation laser line (gamma parameter) [75, 80]. Aligned stacks of images corresponding to the acceptor emission under donor excitation line (FRET image) were first corrected for the above-mentioned parameters. Each pixel of the FRET image was corrected according to the pixel intensity of either donor-excited donor-emission images or acceptor-excited acceptor-emission images Fig. S1). Using the binary masks created before corresponding to post-synaptic terminals, donor and acceptor images, the pixels where the three objects were found overlapping were studied. The percent of pixels where any FRET signal was observed were quantified, allowing us to have a qualitative measure of the occurrence of the FRET effect.

iPSC to cortical neuron differentiation

iPSC lines derived from peripheral blood mononuclear cells from participants in the Lothian Birth Cohort 1936 (LBC1936) were used for this study as previously described

[33, 69, 76]. In this study we used lines EDi030, EDi034, and EDi036. Neuronal differentiation was induced with dual SMAD inhibition (10mM SB431542, [Tocris, 1614] and 1mM dorsomorphin [R&D, 3093/10]) as published previously [61]. After 12 days induction, neuroepithelial cells were passaged mechanically onto 1:100 Matrigel (Corning, 354,230) and maintained in N2B27 media (1:1 of DMEM F12 Glutamax [Thermo Fisher Scientific, 10565018] and Neurobasal media [Thermo Fisher Scientific, 12348017], 1X N-2 (Thermo Fisher Scientific, 17,502–048], 1X B-27 [Thermo Fisher Scientific, 17,504–044], 1mM L-Glutamine [Thermo Fisher Scientific, 25,030–024], 5mg/mL insulin [Merck, I9278-5ML], 100mM 2-mercaptoethanol [Thermo Fisher Scientific, 31350010] 100mM non-essential amino acids [Thermo Fisher Scientific, 11,140–050]), and 1X antibiotic/anti-mycotic [Thermo Fisher Scientific, 15240062]). Neural precursor cells were passaged with accutase (Thermo Fisher Scientific, A11105-01) at day 20, and day 25. A final passage was performed at day 30, with cells plated onto poly-L-ornithine (Merck, P4957) treated glass cover slips coated with 1:100 Matrigel, 10mg/mL laminin (Merck, L2020-1MG), and 10mg/mL fibronectin (Merck, F2006). Between days 35–49 maturing neurons N2B27 was supplemented with 10mM forskolin (Tocris, 1099). From day 50 on N2B27 was supplemented with 5ng/mL BDNF (R&D Systems, 248-BD) and 5ng/mL GDNF (R&D Systems, 212-GD).

Generation of brain homogenate from Alzheimer's patients to challenge iPSC neurons was conducted according to a published protocol [26] with modifications. Human brain tissue was homogenised with a Dounce homogeniser and placed in a low protein binding 15mL tube (Thermo Fisher Scientific, 30,122,216) containing 10 mL 1X artificial CSF (pH 7.4) supplemented with 1 × cOmplete mini EDTA-free protease inhibitor cocktail tablet (Roche, 11,836,170,001) per 10 mL, per 2 g of tissue. The solution was placed on a roller for 30 min to extract soluble proteins, then centrifuged at 2000 RCF for 10 min to remove large, insoluble debris. The supernatant was transferred to ultracentrifuge tubes (Beckman, 355,647) and then centrifuged at 200,000 RCF for 110 min. The resulting supernatant, a homogenate fraction containing soluble Aβ forms, was then transferred to a Slide-A-Lyser G2, 2K MWCO 15mL dialysis cassette (Thermo Fisher Scientific, 87,719) and dialysis was conducted in 1X aCSF with magnetic stirring for three days at 4 °C to remove salts from the homogenate. During this time, the 1X aCSF was exchanged every 24 h. Dialysed brain homogenate was divided into two equal portions in low protein binding 15 mL tubes. Protein A Agarose (PrA) beads (Thermo 20,334) were washed three times in 1X aCSF. 30uL of Washed beads were then added per 1mL of homogenate. To create Aβ− treatment samples, Aβ was immunodepleted by adding 20 µL 4G8 antibody (Biolegend, 800,711) per 1 mL of homogenate and 20 µL 6E10 antibody (Biolegend, 803,001) per 1 mL of homogenate. To create Aβ + treatment samples, homogenate was 'mock-immunodepleted' with isotype control antibodies to non-human antigens by adding 20 µL of GFP (DSHB, DSHB-GFP-12A6) and GFP (DSHB, N86/38) antibody per 1ml of homogenate. Concentration of $A\beta_{42}$was determined by ELISA (WAKO 4987481457102). Homogenate was then incubated for 24 h on a rocker, during which time the Aβ antibody complexes bind to the PrA beads in the immunodepleted portion. After 24 h incubation, homogenate was centrifuged at 2500 RCF for 5 min to remove the beads, and the supernatant was collected. The process of adding beads and antibody/serum to homogenate was repeated twice more. After the third centrifugation step, PrA beads alone were added to both Aβ + and Aβ− homogenate, incubated for 2 hours on a rocker, and then centrifuged at 2500 RCF for 5 min to clear any remaining antibody. Finally, homogenate from each portion was aliquoted at 0.5 mL into 1.5 mL low protein binding Eppendorf tubes (Thermo Fisher Scientific, 0030108116) and stored at − 80 °C. Concentration of Ab1-42 in Aβ + and Aβ− homogenate was quantified by sandwich ELISA (WAKO), according to manufacturer instructions using a ClarioSTAR spectrophotometer (BMG Labtech).

To determine whether Aβ treatments induce cell death, Click-iT™ Plus TUNEL Assay Kits for In Situ Apoptosis Detection (Thermo Fisher Scientific, C10617) was used to detect apoptotic cells according to the manufacturer's protocols. Samples were fixed with 4% formalin (Polysciences, 04018–1), permeabilized with 0.3% Triton-X-100 in 1X PBS for 20 min at room temperature, incubated with TUNEL reaction buffer for 10 min at 37 °C, incubated with TUNEL reaction mixture for 1 h at 37 °C, blocked with 3% bovine serum albumin, and incubated with TUNEL reaction cocktail for 30 min at 37 °C. Immunocytochemisty was then performed for co-staining. All incubations were conducted in the dark.

Neurons from three iPSC donors were grown to approximately day 200 post-induction in 24 well plates. Cells were treated with media, Aβ + homogenate, or Aβ− homogenate diluted 1:4 in media for 24 h followed by addition of CT1812 (10 mM) or DMSO (Merck, D2438-50ML) vehicle treatment for a further 24 h. The final concentration of Aβ in the Aβ + treatment condition was 90 pM and in the Aβ− condition it was 8 pM. Cells were pre-incubated with Aβ + homogenate for 24 h before CT1812 treatment to model the human treatment condition in which people have Aβ accumulation before treatment with CT1812 begins. RNA was harvested from four pooled wells per treatment condition using trizol-chloroform extraction. Remaining coverslips were fixed for immunocytochemistry (ICC) as below. Each experiment was repeated with three different differentiations of each of the three lines.

Cells for ICC were fixed with 4% formalin (Polysciences, cat.04018–1) for 15 min, Washed thrice in 1X phosphate buffered saline (PBS). Fixed cells were permeabilized and blocked with in 1X PBS with 0.3% Triton-X and 3% bovine serum albumin (permeabilising block solution) for 30 min. Coverslips were incubated overnight at 4 °C with primary antibodies TMEM97, homer1, MAP2, GFAP, and Tuj1. Cells were washed with 1X PBS, and incubated in secondary antibodies diluted 1:500 in permeabilising block solution for 1 h in the dark. For the detailed information of the primary and secondary antibodies used, please see Table S2. Cells were incubated with 1:10,000 DAPI in 1X PBS with 0.3% Triton-X for 10 min, and washed 2 × in 1X PBS. Coverslips were mounted on slides (VWR, 631–0847) with mounting media (Merck, cat.345789-20ML) and imaged on a Leica TCS confocal microscope with an oil immersion 63 × objective.

For calcium imaging, cells were incubated for 7 days from approximately day 190 post-differentiation in GCamP6s AAV (pAAV.Syn.GCaMP6s.WPRE.SV40, Addgene 100843-AAV1). Images were acquired on an Leica DMI6000B inverted fluorescence microscope (20X objective, 2 frames per second). For acute treatments, cells were imaged at baseline followed by 2.5 min of treatment with Aβ + homogenate, Aβ− homogenate, 10 µM CT1812 or DMSO vehicle followed by repeat imaging of the same sites. For 24 h treatments, cells were incubated in Aβ + homogenate, Aβ− homogenate, or media for 24 h followed by baseline imaging, 2.5 min treatment with 10 µM CT1812 or DMSO vehicle, and re-imaging of the same sites.

RNA sequencing was performed on total RNA samples using TruSeq stranded mRNA-seq library preparation along with next-generation sequencing on NovaSeq6000 platform; sequencing was carried out by Edinburgh Genomics (Edinburgh, UK). Samples were sequenced to a depth of approximately 100 million 50-base pair, paired-end reads. The reads were mapped to the primary assembly of the human (hg38) reference genome contained in Ensembl release 106, using the STAR RNA-seq aligner, version 2.7.9a [18]. Tables of per-gene read counts were generated from the mapped reads with featureCounts, version 2.0.2 [39]. Differential gene expression was performed in R using DESeq2, version 1.30.1 [40]. Gene ontology analyses were run on the Gene Ontology online resource using their Panther online search tool for Biological Processes (http://geneontology.org/). MetaCore + MetaDrug version 22.3 build 71,000 was used to perform pathway analysis on Abeta vs. Vehicle, and Abeta + Drug vs. Abeta + Vehicle conditions (unadjusted p value < 0.05). STRING (Version 11.5) pathway analysis of Abeta + Drug vs. Abeta + Vehicle conditions (unadjusted p value < 0.05) [81].

ELISA quantification of Aβ content in synaptoneurosomes

$A\beta_{40}$ and $A\beta_{42}$ content was quantified in total homogenate and synaptoneurosome fractions of control and AD cases reported in Table 1. Total homogenate and syanptoneurosomes were prepared from BA20/21 tissue as described previously [33]. Total protein was quantified with micro Bicinchoninic acid assay (Pierce, UK). $A\beta_{40}$ content was quantified using serial dilutions of samples with Thermo Fisher KHB3481 Aβ 40 human ELISA kit following manufacturer's instructions. $A\beta_{42}$ content was quantified using serial dilutions of samples with Thermo Fisher KHB3441 Aβ 42 human ELISA kit or KHB3544 ultrasensitive Aβ 42 human ELISA kit (one sample to confirm values below sensitivity threshold) following manufacturer's instructions. Values obtained for sample dilutions within the linear range of standard curve were multiplied by dilution factor, averaged, and divided by total protein content, yielding one value per case in pg/mg of total protein.

Statistical analysis

Brain weight, age at death, $A\beta_{42}$ levels, $A\beta_{40}$ levels, $A\beta_{42/}A\beta_{40}$ ratios, and PMI differences between groups were analysed with t test or Wilcoxon test depending on the Shapiro–Wilk Normality test results. Sex, *APOE* genotype, Braak stage and Thal phase were analysed with Fisher-exact tests. The comparison between groups in all the other studied variables was analysed using linear mixed effects models including case or cell line as a random effect to account for multiple measures. Sex, age, APOE4 status, Braak stage, Thal phase and PMI were included as a fixed effects in the initial statistical models for human post-mortem data followed by sequential removal of fixed effects to find the model that best fit the data for our primary question of whether Aβ and TMEM97 are found within the same synapses. The linear mixed effects model including only diagnosis as a fixed effect and sample nested in case as a random effect was the best fit for the data as assessed with the Akaike Information Criteria (AIC) [9]. Despite the model including sex being a slightly poorer fit, we appreciate that inclusion of sex as a biological variable is best practice in dementia research [42], so sex remained in the model. Including an interaction between sex and diagnosis was a better fit than without the interaction, thus our final statistical model applied in the study was diagnosis*sex + (1|case/sample). For analysis of the effect of plaque proximity, distance from plaque was included as a fixed effect in the model. ANOVAs and Tukey corrected post-hoc were run on the linear mixed

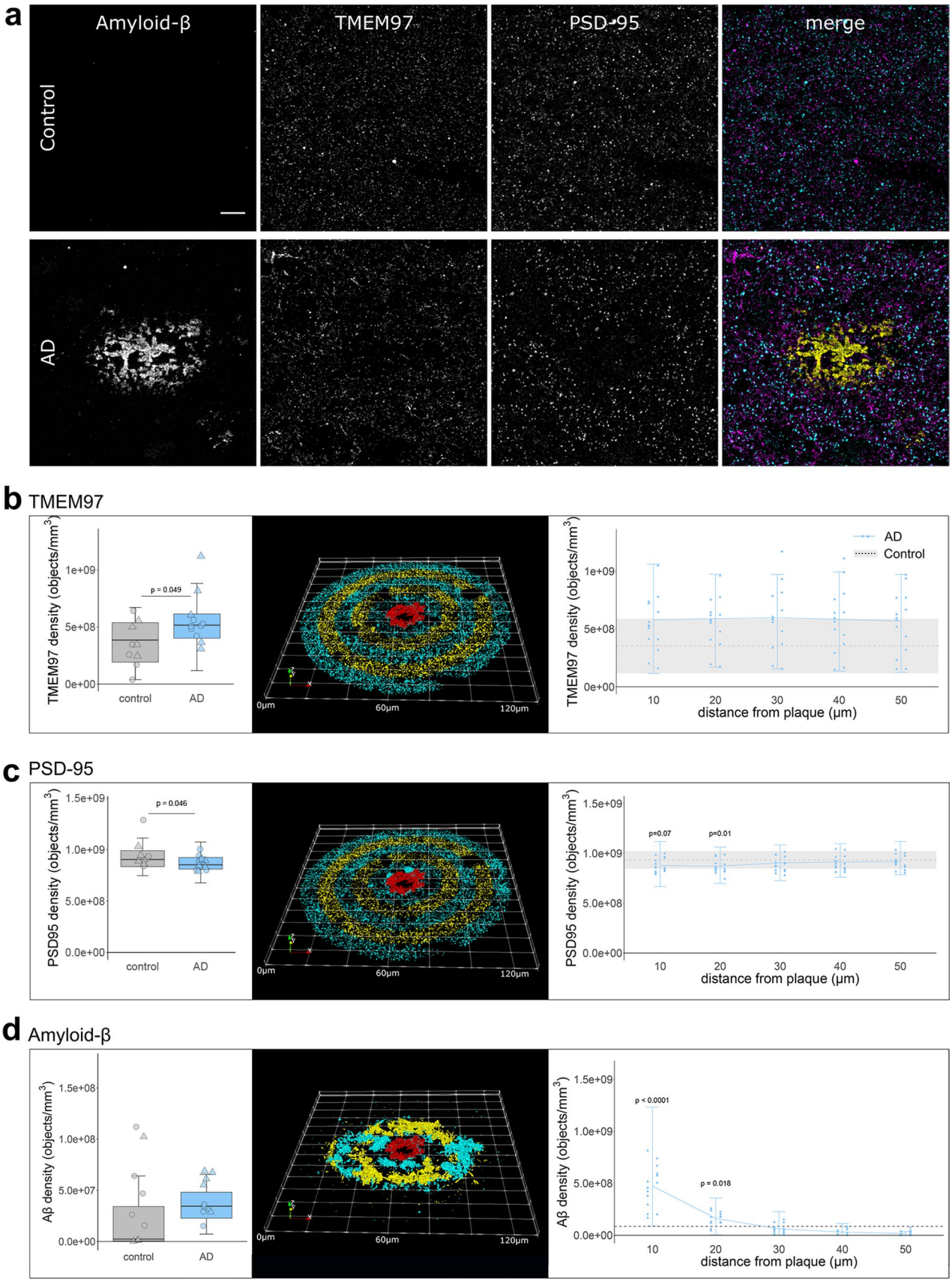
a
Amyloid-β
TMEM97
PSD-95
merge
Control
AD
b TMEM97
TMEM97 density (objects/mm3)
p = 0.049
control
AD
0µm
60µm
120µm
AD
Control
distance from plaque (µm)
c PSD-95
PSD95 density (objects/mm3)
p = 0.046
p=0.07
p=0.01
d Amyloid-β
Aβ density (objects/mm3)
p < 0.0001
p = 0.018

◂**Fig. 1** Immunoreactivity pattern and density of TMEM97, Aβ and PSD95. **a** representative maximum intensity projection images of ten consecutive 70 nm-thick sections from a control and an Alzheimer's case. Immunoreactivity against Aβ (6E10, yellow), TMEM97 (magenta) and PSD95 (cyan) is shown. Overall density (left) or the density in relation to Aβ plaque cores (right) of TMEM97 (**b**), PSD95 (**c**) and Aβ (**d**) is plotted. The 3D reconstructions were made from 19 consecutive sections of a representative Alzheimer's case. The Aβ core is shown in red and the objects distributed every 10um bins are coloured. Scale bar represents 10 µm. Boxplots show quartiles and medians calculated from all image stacks in the study. Data points show case means (females, triangles; males, circles). *p* values on left panels show significant effect of disease (ANOVA after linear mixed effects model). On right panels, *p* values show Tukey corrected post-hoc significant differences between 50 µm and the indicated plaque distance in the AD data. In D, note the scales are different in the two plots as there is an order of magnitude more Aβ near plaques than when averaged across all images

effects models to determine differences between groups. Where the residual plots indicated a poor fit of the raw data in the linear mixed effects models, Tukey transformations of the data were conducted to improve the model fit. All the analyses were performed with R v4.1.2 [53] and the scripts and full statistical results can be found at https://datashare.ed.ac.uk/handle/10283/3076.

Rigour in study design

The immunostaining, image acquisition, image processing and analyses were performed blinded to the clinicopathological diagnosis. Mice were randomly assigned to treatment groups and treated by blinded experimenters. Bias was also minimized by setting the same parameters for image acquisition and image analysis for all the included cases.

Results

Characteristics of human cases

We used human post-mortem brain samples from inferior temporal gyrus (BA20/21) to investigate proximity of Aβ and synaptic proteins. Details of human cases included are shown in Table 1. Our Alzheimer's and control cohorts are age (Wilcoxon test $W = 29.5$, $p = 0.13$) and sex matched ($p = 1$ Fisher's exact test) and matched for *APOE4* allele status (Fisher's exact test $p = 0.41$). Post-mortem interval (PMI) was slightly longer in Alzheimer's group (Welch's *t* test, $t = -2.36$, $p = 0.030$). Both Braak stage and Thal phase were higher in AD than control group due to our inclusion criteria for the groups ($p < 0.01$ Fisher's exact tests).

TMEM97 levels are increased in Alzheimer's post synapses

We used array tomography to examine synaptic localisation of Aβ, TMEM97 and other potential binding partners. Image stacks were acquired in areas containing amyloid plaques where we previously demonstrated the highest amount of synaptic Aβ. The overall density of TMEM97 positive objects was assessed in the temporal cortex revealing an immunoreactivity pattern of a membrane protein, with widespread presence in grey matter in both Alzheimer's and control cases (Fig. 1A). The density of TMEM97 objects was significantly higher in Alzheimer's than control cases (fold increase: 1.56; effect of disease $F[1,19.36] = 4.41$, $p = 0.049$, no significant sex differences). This increase was not related to the proximity of an Aβ plaque (Fig. 1B). As previously described [34], post-synaptic terminal density was reduced in AD (Fig. 1B, 7% reduction in PSD density $F[1,28.73] = 4.36$, $p = 0.046$, no significant sex differences). Postsynaptic puncta density was further reduced in the vicinity of Aβ plaque cores of Alzheimer's cases (effect of plaque distance $F[4,Inf] = 4.44$, $p = 0.001$, no sex effect, Fig. 1C). As expected, Aβ object density was elevated close to Aβ plaques (effect of plaque distance $F[4,Inf] = 47.86$, $p < 0.0001$; Fig. 1D).

TMEM97 and Aβ are found in a higher proportion of synapses in Alzheimer's

We recently described an increase of TMEM97 protein levels in biochemically isolated synaptic fractions from Alzheimer's brain compared to controls [25], and in multiple previous studies we and others have observed increased levels of in Aβ synapses [29, 34]. In the present study, we confirmed biochemically that both $Aβ_{40}$ and $Aβ_{42}$ levels are increased in synaptic fractions of AD brain (Fig. S2). Further, we were able to visualize the synaptic localization of TMEM97 and Aβ using array tomography. The analysis of over 1 million individual synaptic terminals revealed an increased proportion of synapses with TMEM97 in Alzheimer's when compared to healthy controls (fold increase: 2.10; effect of disease $F[1,20.16] = 5.67$, $p = 0.027$, Fig. 2). There were no sex effects in the proportion of synapses containing TMEM97. In line with the hypothesis that TMEM97 is a binding partner of Aβ, we found that Aβ was present in post-synaptic terminals (effect of disease $F[1,21.86] = 7.56$, $p = 0.011$, Fig. 2). Interestingly, there was a significant interaction between disease and sex in the proportion of synapses with Aβ (disease* sex interaction $F[1,21.86] = 5.1$, $p = 0.034$) with female subjects having more synaptic Aβ. Importantly, that Aβ was found overlapping TMEM97 immunoreactivity in the same post synapses (effect of disease $F[1,20.66] = 19.72$, $p = 0.0002$, Fig. 2).

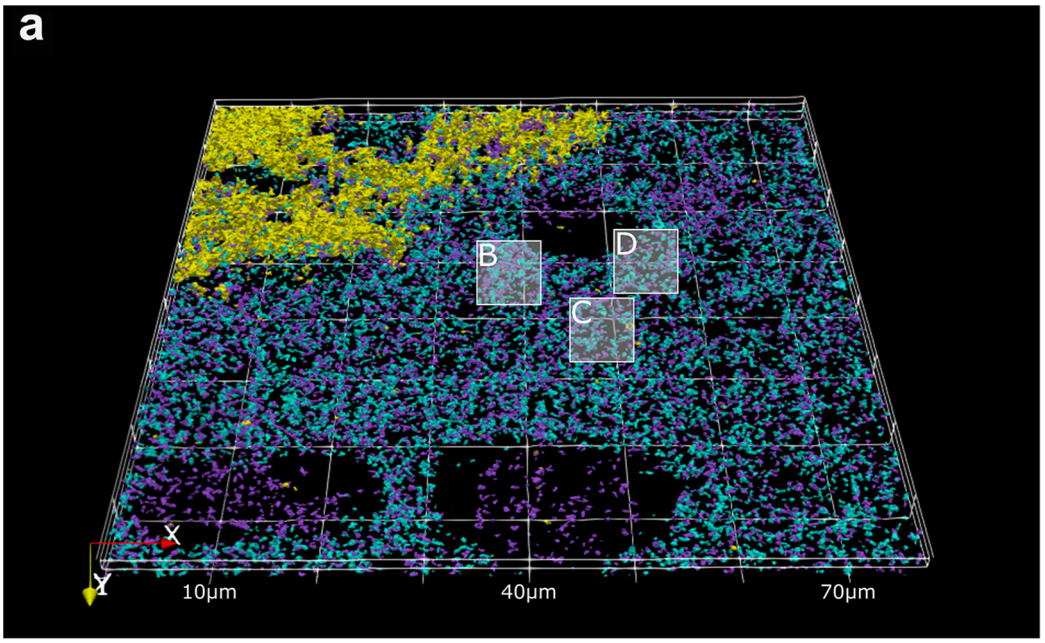
a
B
C
D
X
Y
10µm
40µm
70µm

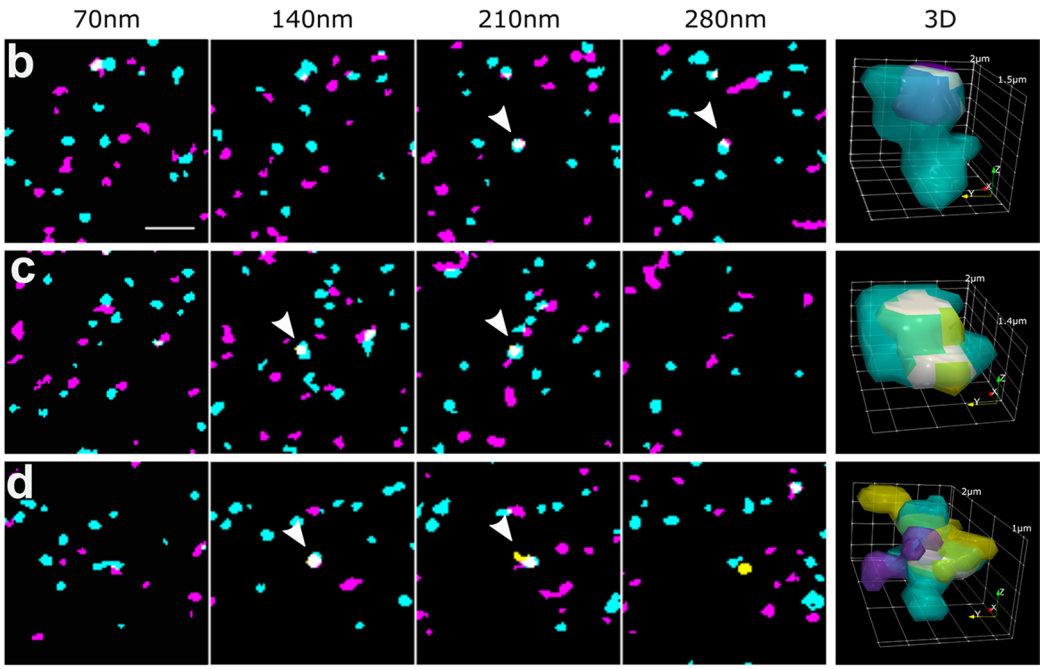
70nm
140nm
210nm
280nm
3D
b
c
d
2µm
1.5µm
1.4µm
1µm

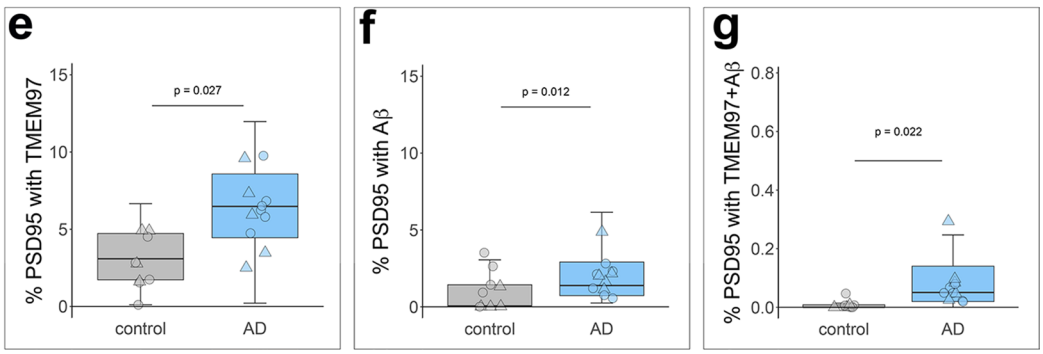
e
% PSD95 with TMEM97
p = 0.027
control
AD
f
% PSD95 with Aβ
p = 0.012
control
AD
g
% PSD95 with TMEM97+Aβ
p = 0.022
control
AD

◂**Fig. 2** TMEM97 is found at higher levels in Alzheimer's synaptic terminals compared to healthy controls. 3D reconstructions were made from 20 consecutive 70 nm-thick sections from a representative Alzheimer's case stained for Aβ (6E10, yellow), TMEM97 (magenta) and PSD95 (cyan). In the top 3D reconstruction (**a**), three white boxes label the magnified regions that highlight: a PSD95 terminal with TMEM97 (**b**), a post-synaptic terminal with Aβ (**c**) and a PSD95 synaptic terminal with both Aβ and TMEM97 (**d**). In magnified images (**b**–**d**), four consecutive sections from the image stack are shown (each 70 nm apart). White arrowheads indicate synaptic localization and a 3D reconstruction (right panel) of the pointed synapse where colocalization is observed (white). Box plots show the percent of post-synaptic terminals that contained TMEM97 (**E**), Aβ (**F**), or both (**G**), in Alzheimer's and control cases. Boxplots show quartiles and medians calculated from each image stack. Each data points refers to the means of a single human tissue donor (females, triangles; males, circles). *p* values show ANOVA after linear mixed effects models. Scale bar: 2 µm

Synaptic TMEM97 and Aβ are close enough to generate a FRET signal

After confirming the presence of TMEM97 together with Aβ in synapses of Alzheimer's cases, and given the ability of Sigma-2 receptors to displace Aβ from neuronal synapses [27], we assessed the proximity of the immunoreactivity of TMEM97 with that of Aβ in synapses of AD cases by FRET. In this single pixel analysis, those areas where the donor (labelling Aβ) and the acceptor (labelling TMEM97) were found overlapping within a PSD95 positive object were quantified in the corrected donor excitation-acceptor-emission image (Fig. S1 and methods for further details). This quantification allowed us to detect FRET only when both donor and acceptor were present in synapses and within approximately 10nm of each other. To determine limitations of the technique, we measured the residual FRET signal in stacks where only the donor or the acceptor was labelled as negative controls, and the maximum FRET signal was determined where the donor and acceptor labelled the same target as the positive control (Fig. 3, green shading on the plot shows the experimental window of detecting FRET signal between negative and positive control levels).

In Alzheimer's cases, we found that in both post and pre synapses where donor and acceptor were present, Aβ labelled with 6E10 antibody and TMEM97 were close enough to generate a FRET signal (Fig. 3). In post synapses, we also observed FRET between Aβ and PrP_c—which has also been observed to bind Aβ in model systems[62]—and between TMEM97 and PGRMC1 which are known to be binding partners in vitro and in human cases [55], and between TMEM97 and PrP_c (Fig. 3). Confirming cellular localization of Aβ to synapses, we saw positive FRET signal between Aβ and PSD95 (Fig. 3). This is in support of findings by other groups in which Aβ has been described to interact in some synapses, including in rat neuronal cultures [28] and our previous study using a similar FRET approach in APP/PS1 mice [35, 50, 52]. We confirmed that TMEM97 generates a FRET signal with oligomeric Aβ in both pre and post synapses using NAB61 to label oligomers and fibrillar oligomers of Aβ (Fig. 3).

To confirm that this effect was not occurring in all areas where donor and acceptor are present in the same pixel, we used a biological negative control looking for FRET between PSD95 and synaptophysin which are close but not interacting as they are separated by the synaptic cleft. As expected, there was not a significant FRET signal between these pre and post-synaptic proteins. There was also no FRET signal between PGRMC1 and PSD95 (Fig. 3). In summary, our FRET experiments confirm close proximity within synapses of Aβ and TMEM97, Aβ and PrP_c, TMEM97 and PrP_c, TMEM97 and PGRMC1 and Aβ and PSD95, but not PSD95 and synaptophysin or PSD95 and PGRMC1, which are robust as both technical and biological negative controls do not show FRET signal.

TMEM97 modulator reduces synaptic TMEM97-Aβ FRET signal in a mouse model of Alzheimer's

Results from human brain observations suggested that TMEM97 may be a binding partner of Aβ. To determine whether this synaptic binding is reversible in vivo, we used the Sigma-2/TMEM97 receptor complex allosteric modulator CT1812—currently in clinical trials for Alzheimer's [11, 21]—in a recently described Alzheimer's mouse model [51]. APP/PS1 + Tau mice (APP-PS1 ±; MAPT -/-; CKTTA +; Tg21221) and littermate controls were treated with either vehicle ($n = 10$ APP/PS1 + Tau, $n = 10$ control) or CT1812 (10 mg/kg/day given orally, $n = 10$ APP/PS1 + Tau, $n = 10$ control), which selectively binds to the Sigma-2 (TMEM97) receptor complex (Fig. 4). The dose delivered to mice was based on our previous study in which the same dose and treatment duration caused recovery in memory in a plaque-bearing mouse model [28].

We first estimated the percent receptor occupancy of CT1812 in brain, which was calculated based on the measured brain concentration of the drug (see methods and [27]). We observed a statistically significant sex difference in the percent of estimated receptor occupied by the drug. Male APP/PS1 + Tau mice had an average of 85.13 ± 6.4% estimated receptor occupancy, while females had an average of 69.69 ± 11% ($\beta = 15.44$; $p < 0.001$, Fig. 4B). The increase in drug estimated receptor occupancy in male mice was observed in both genotypes ($\beta = 44.63$; $p = 0.006$, Supplementary Fig S3). This difference could not be explained by any experimental procedures as all animals were given the same dose of compound from the same stock. Body weight, which could affect drug uptake, did not differ between treatment groups ($F[1, 36] = 0.74$, $p = 0.40$), but body weight was different between male and female mice with males

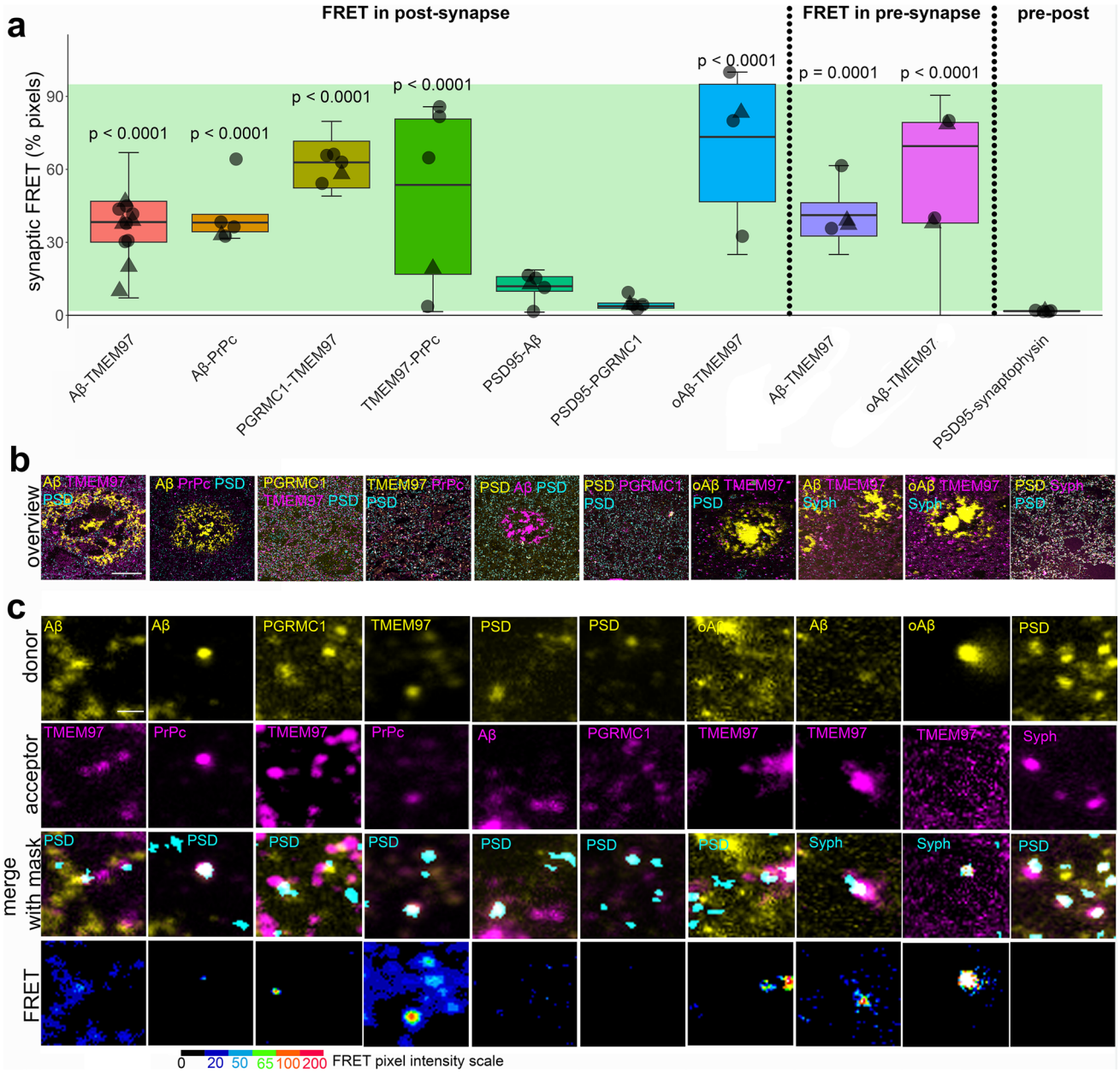

Fig. 3 Aβ and TMEM97 are close enough at the Alzheimer's synapses to generate a FRET effect. Pixels where pairs of interest were colocalized within synaptic puncta were analysed to determine whether they generate a FRET signal. The percent of synaptic pixels where FRET signal was detected by each protein pair are plotted (**a**). The green bar in the boxplot shows the window of detecting FRET signal defined by the positive control signal where an acceptor fluorophore was applied to the same protein as the donor fluorophore using a tertiary antibody (top) and negative controls where no acceptor fluorophore was present (bottom). Boxplots show quartiles and medians calculated from each image stack. Data points show case means (females, triangles; males, circles). *p* values show post-hoc Tukey corrected differences between the pair indicated and the biological negative control of PSD-synaptophysin FRET. Images in panel **b** show a maximum projection of five consecutive sections showing a 100×100 µm overview of the donor channel (yellow) acceptor channel (magenta) and the synaptic channel segmented in three dimensions used as region of interest for FRET (cyan) for each FRET pair used in the study. Panel **c** shows 5×5 µm regions containing examples of donor and acceptor staining in synaptic masks and the generated FRET signal in a single section with intensity represented by colour as in colour scale. Scale bars: 20 µm in **b**, 1 µm in **c**

being heavier (F[1, 36] = 62.33, $p < 0.0001$). There was no treatment:sex interaction in analysis of body weight nor was there a significant difference in the numbers of male vs female mice in the different treatment groups (Fisher test $p = 1$, 95% CI = 0.30, 5.04). The treatment of non-transgenic control mice did not affect the density of Aβ, Tau or PSD95 (Supplementary Fig S2A-B), confirming that treatment with this compound was not synaptotoxic. CT1812 treatment

in transgenic mice did not change plaque burdens but did reduce astrogliosis in hippocampus (Supplementary Fig S4).

Since it has been reported that drug concentrations above 80% estimated receptor occupancy are effective and concentrations lower than 60% were ineffective [27], the effect on synaptic TMEM97 and Aβ localization was studied on the mice that reached an 80% estimated receptor occupancy threshold ($n = 5$ APP/PS1 + Tau mice, Table S1). CT1812 did not statistically significantly influence the overall densities of Aβ, TMEM97 or PSD95 nor the synaptic localization of Aβ and/or TMEM97 (Fig. 4A,C,E). When we modelled the effect of treatment and sex on the synaptic FRET signal between Aβ and TMEM97, we did not observe a significant difference between groups (vehicle mean 52.8 ± 12%; treated mean 44.2 ± 5.61%, Fig. 4D). However, the increase of estimated receptor occupancy by the drug significantly correlated with a decrease of synaptic FRET signal between Aβ and TMEM97 (rho = − 0.94, $p = 0.017$, Fig. 4F).

Taken together, we found that in the CT1812 treated APP/PS1 + Tau mice with estimated receptor occupancy in the therapeutic range, there was a decreased synaptic FRET signal between Aβ and TMEM97, indicating increased distance between the two proteins.

TMEM97 modulator ameliorates Aβ–induced phenotypes in human iPSC neurons

To investigate whether disrupting TMEM97-Aβ interactions protects living human neurons, human iPSC-derived neurons were challenged with the soluble fraction of Alzheimer's brain homogenate or identical homogenate immunodepleted for Aβ and treated with CT1812 or vehicle to investigate whether disrupting TMEM97-Aβ interactions protects living human neurons. Brain homogenates were added to neuronal media at final concentrations of 90 pM of Aβ in the mock-immunodepleted condition and approximately 8 pM in the immunodepleted condition (detection was at the lower limit of ELISA sensitivity). Immunocytochemistry confirms that TMEM97 is present in homer positive post synaptic puncta in dendritic spines and that when treated with Aβ-containing brain homogenate, Aβ also accumulates in synapses (Fig. 5A). Both cell counts and TUNEL assay showed that the brain homogenate treatments were not cytotoxic compared to media (Fig. 5B, C), which is important as we wish to model synaptic damage, not neuron death, since oligomers of Aβ at physiological concentrations in human brain are thought to cause synaptic damage and not to induce neuron death directly. Cytotoxicity was generally low (< 10%) in all conditions. To confirm that our iPSC-derived neurons were active and look for functional effects of challenging with Aβ containing homogenates and drug treatments, we used calcium imaging after loading neurons with GCaMP6 virus (Supplementary Figure S5). Images of GCaMP6 fluorescence show that neurons were active in all conditions. Quantification of the peak frequency of GCaMP normalized to the baseline condition for each group shows that acute treatment with homogenate or drug does not change between Aβ + or Aβ + homogenate or CT1812 or vehicle. However, both human brain homogenate treated groups are lower than the control (vehicle treatment; Tukey-corrected post-hoc test after linear mixed effects model, $p < 0.0001$) indicating that exposure to human brain homogenate affects cell function. Pre-incubation with homogenate for 24 h before CT1812 or vehicle treatment induced a significant interaction between Aβ status of the homogenate and drug treatment ($F[1,257] = 9.06$, $p = 0.003$) with a significant decrease in peak frequency between Aβ–incubation followed by vehicle treatment and Aβ + followed by CT1812 treatment.

RNA sequencing was used to determine gene expression changes after exposing cells to human Alzheimer's brain homogenate containing soluble Aβ and CT1812 or vehicle. Treatment with Alzheimer's brain homogenate containing soluble Aβ induced over 4000 differentially expressed genes compared to media treatment. The difference between Aβ− and Aβ + homogenate was much smaller with only 7 differentially expressed genes (adjusted p value < 0.05), 3 upregulated and 4 downregulated (Fig. 5D). Treatment with CT1812 did not significantly change expression of these 7 genes compared to vehicle after Aβ + homogenate. Although not statistically significant, the fold changes of these 7 genes largely changed in the opposite direction with treatment with CT1812 (Table S3). Three of the genes upregulated by Aβ + homogenate challenge are expressed in neurons and implicated in neurodegenerative diseases (DYS—dystonin, SACS—sacsin, and VPS13C—vacuolar protein sorting 13). Eight genes were differentially expressed with CT1812 treatment after Aβ + homogenate challenge (Fig. 5E, Supplementary Table 3). Several of the transcripts regulated by CT1812 are expressed in astrocytes, which are observed in small numbers in our cultures (averaging 16% GFAP positive cells in the 200 day old cultures used, Fig. 5F). One of the transcripts significantly changed by CT1812 treatment, CHI3L1, which encodes YKL-40 protein, is expressed in astrocytes and is an interesting biomarker of inflammation in Alzheimer's disease [48].

Although only a handful of transcripts reached a statistically significant change after correcting for multiple testing, pathway analysis using a less strict criteria of $p < 0.05$ unajdusted p values to look for patterns of expression changes using MetaCore, revealed enrichment of immune/inflammatory pathways with Aβ treatment compared to immunodepleted Aβ treatment. These included the JAK/STAT pathway known to be involved in astrocyte differentiation and function, indicated by Leukemia Inhibitory Factor (LIF) and Leukemia Inhibitory Factor Receptor (LIFR) enrichment, a known pro-inflammatory cytokine involved

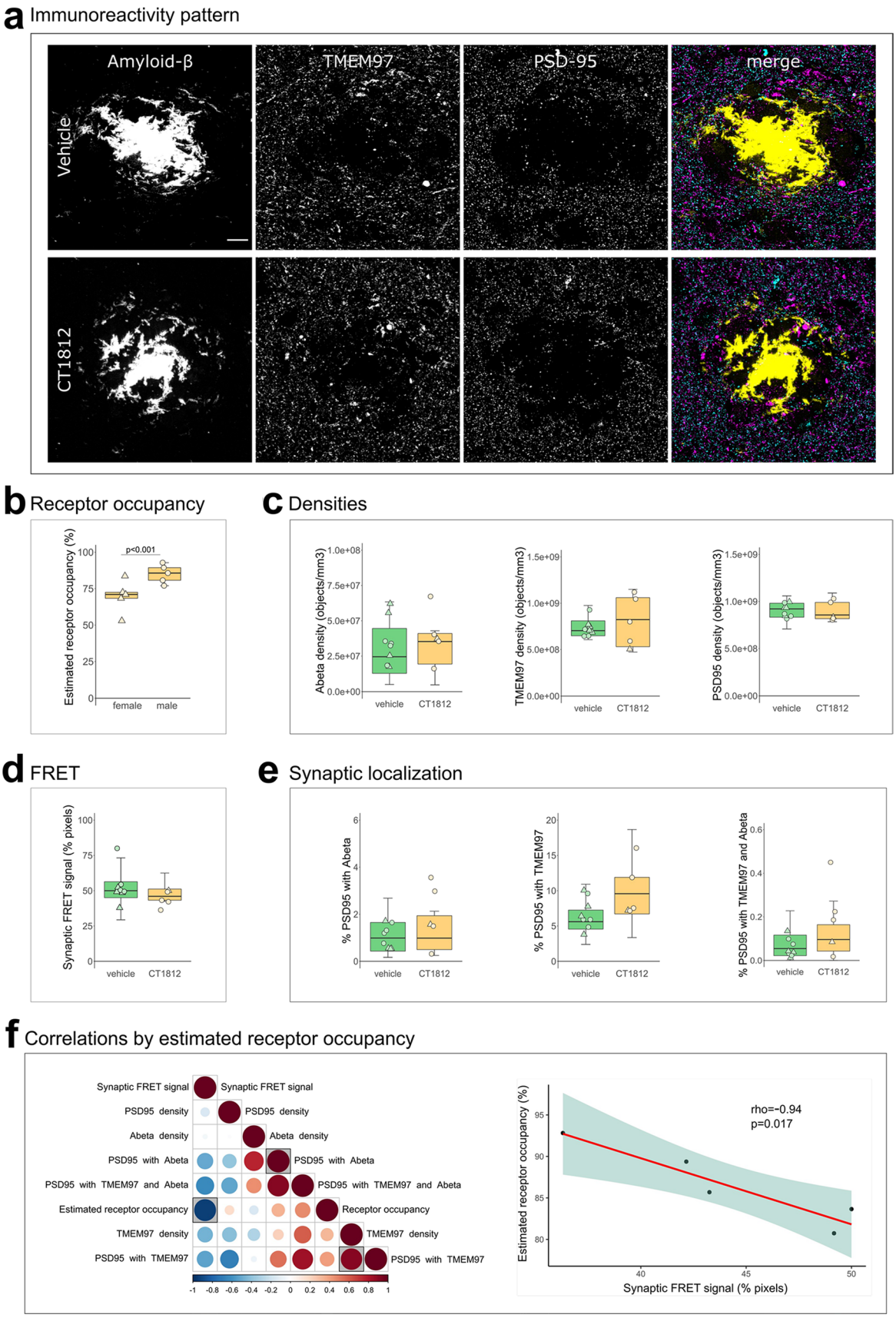
a Immunoreactivity pattern
Amyloid-β
TMEM97
PSD-95
merge
Vehicle
CT1812
b Receptor occupancy
Estimated receptor occupancy (%)
p<0.001
female
male
c Densities
Abeta density (objects/mm3)
TMEM97 density (objects/mm3)
PSD95 density (objects/mm3)
vehicle
CT1812
d FRET
Synaptic FRET signal (% pixels)
e Synaptic localization
% PSD95 with Abeta
% PSD95 with TMEM97
% PSD95 with TMEM97 and Abeta
f Correlations by estimated receptor occupancy
Synaptic FRET signal
PSD95 density
Abeta density
PSD95 with Abeta
PSD95 with TMEM97 and Abeta
Estimated receptor occupancy
Receptor occupancy
TMEM97 density
PSD95 with TMEM97
rho=-0.94
p=0.017
Estimated receptor occupancy (%)
Synaptic FRET signal (% pixels)

◂**Fig. 4** Effect of TMEM97 modulator on synaptic Aβ and TMEM97 in the APP/PS1 + Tau mouse model. Representative images of immunoreactivity patterns found in vehicle or CT1812 treated mice are shown in **a**. Images show maximum intensity projections of 16 consecutive 70nm-thick sections of cases stained for Aβ (yellow), TMEM97 (magenta) and PSD95 (cyan). **b**, the estimated percent of receptor occupancy by the drug in the CT1812-treated group. **c,** quantification of overall densities of the three studied proteins. **d**, the percent of synaptic pixels that contain both Aβ and TMEM97, and FRET signal. **e**, the post-synaptic terminals localisation of Aβ, TMEM97, or both. **f**, Correlations were estimated between measured parameters and a correlation matrix of the assessed variables is shown (left panel) in which the colour and size reflect the rho (scale below the plot) and the statistically significant correlations are highlighted with a shaded square. The correlation between percent estimated receptor occupancy and percent of synaptic FRET signal (right panel) displaying the regression line (red), the 95% confidence interval (green) and the Spearman correlation results (rho, *p* value). Scale bar: 10μm. Boxplots show quartiles and medians calculated from each image stack. Data points refer to case means (females, triangles; males, circles). Analysis with linear mixed effects models including treatment group and sex interaction

in the differentiation of neuronal precursor cells into astrocytes (Fig. 5F). STRING (Version 11.5) protein interaction analysis of Aβ + Drug vs. Aβ + Vehicle conditions (unadjusted p value < 0.05) confirmed the findings of TMEM97 localization to synapses. The top 8 GO Components (sorted by strength) were involved in synaptic biology (Fig. 5G). Further, "Synapse" was the top UniProt Keyword of the Aβ + Drug vs. Aβ + Vehicle (unadjusted $p < 0.05$), with a strength of 0.54 and a FDR of 0.00019. Further, biological pathways changed by CT1812 vs vehicle treatment after challenge with Aβ homogenate include several processes important for synaptic function (Supplementary Table 4). Overall, differential expression data and functional imaging support a localization of Sigma-2 receptor at the synapse, and suggest a role for CT1812 in modulating inflammatory pathways, perhaps indirectly by glia that may detect changes in synapse health or activity.

Discussion

In the present study, we visualized TMEM97 within individual synapses in human brain. In Alzheimer's brain, TMEM97 levels were increased in synapses, and TMEM97 was found in close enough proximity to Aβ to be binding. Further we confirm in mouse and human iPSC models that Aβ is in close proximity to TMEM97 in synapses and that CT1812 treatment to disrupt this interaction is beneficial.

TMEM97 (Sigma-2) has been previously linked to Alzheimer's, through in vitro and in vivo pharmacological modulation studies and with regard to a change in expression levels on synapses in Alzheimer's patients. More specifically, in cellular models, treatment with modulators or knocking out Sigma-2 receptor (S2R) constituents TMEM97 or the co-receptor PGRMC1 reduces the internalization of Aβ [27, 54]. In an animal model with Alzheimer's-like plaque deposition, TMEM97 (Sigma-2) modulators improved cognitive deficits [27, 77]. In human cases, we observed TMEM97 is increased in biochemically isolated synapses of Alzheimer's patients compared to age-matched controls, using an unbiased proteomic approach [25]. Those findings and the fact that TMEM97 modulators are pharmacologically well studied, have brought the use of TMEM97 modulators into Phase II clinical trials for Alzheimer's treatment [11, 21].

However, the relationship between Aβ and TMEM97 in human synapses was not previously clear. Our current results support a mechanistic explanation that includes a potentially direct interaction between Aβ and TMEM97, as suggested by the FRET findings (Fig. 6). Importantly, we found that this potential interaction may occur at the synapses, believed to be the earliest affected structure in the context of Alzheimer's and the best pathological correlate of the characteristic cognitive decline [17, 56, 67]. Taken together, these findings link a therapeutic target (TMEM97) with a suspected pathological peptide (Aβ) in a key cellular structure (the synapse).

The relationship between Aβ and synapses has been widely studied [19, 71]. It has been shown that Aβ can be found in synapses of Alzheimer's cases [6, 29, 34, 51, 65, 66], but the mechanisms by which Aβ induces synaptic toxicity remain unclear. The study of synaptic binding partners of Aβ yielded many candidates—reviewed in [30, 46, 63]. The most studied binding partner is the PrP_c, which through a cascade involving a complex with mGluR5 may lead to toxicity independently or via tau [37, 62, 72, 79]. Other binding partners that have been suggested to bind Aβ include the α7-nicotinic receptor [49], Ephrin A4 (EphA4) [73], PSD95 [35, 50, 52] or LilrB2 [32]. It is likely that Aβ is in fact interacting with more than one protein [62]. Due its hydrophobic nature, Aβ binds to lipid membranes interrupting membrane fluidity and destabilizing several membrane receptors [38]. It is relevant to note that most binding partners have not been studied in human brain nor using human derived Aβ species [38, 63]. Further, while Aβ fibrils bind non-specifically to a variety of surfaces, and Aβ monomers bind to several receptors when applied exogenously [5], Aβ oligomers have been shown to bind saturably to a single site[27, 62] suggesting specific pharmacological interactions with receptors. Therefore, it has been tricky to determine which Aβ binding partners are relevant in living human brain. The structural state of Aβ labelled with 6E10 antibody(monomer, oligomer or fibril) recognised in the present array tomography studies is not clear, which is a limitation of the study, but we have confirmed the interaction of TMEM7 with NAB61, an antibody that preferentially recognises fibrillar oligomers and reacts with synaptic oligomeric Aβ [34]. Within the limitations of the technique, we are able to observe proximity of synaptic proteins to a degree that has

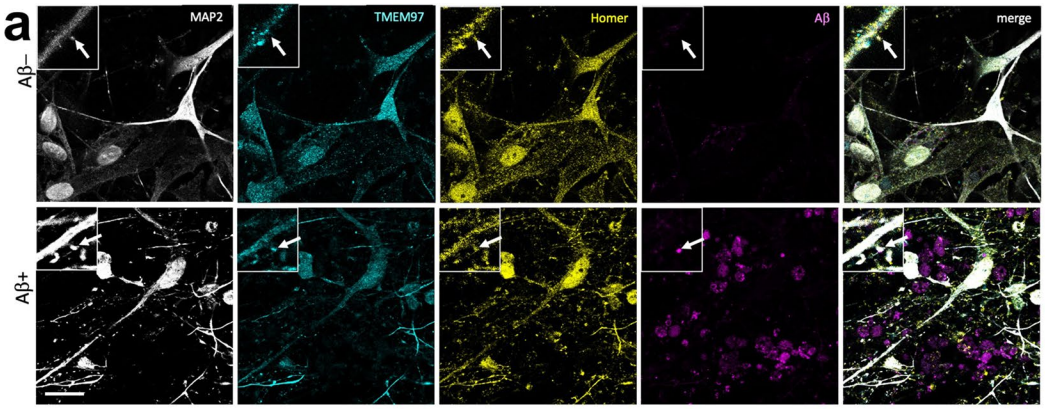

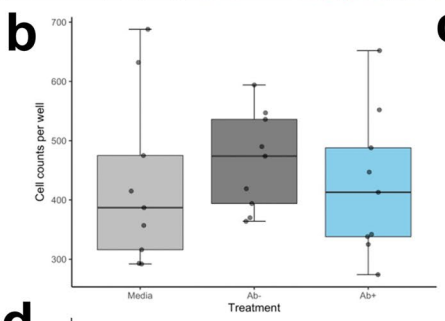

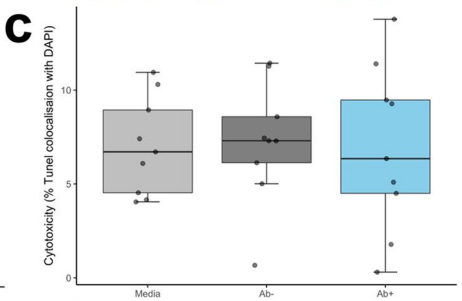

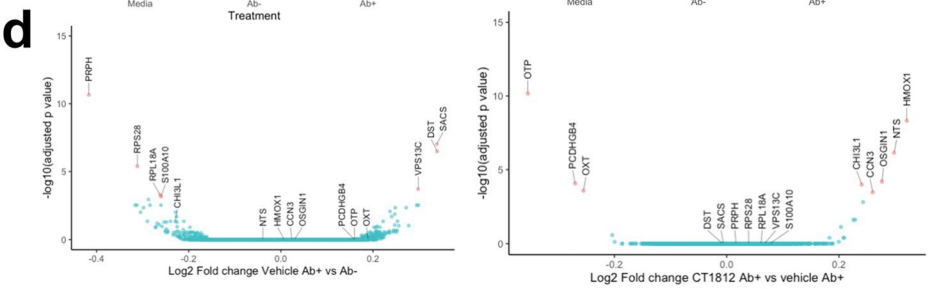

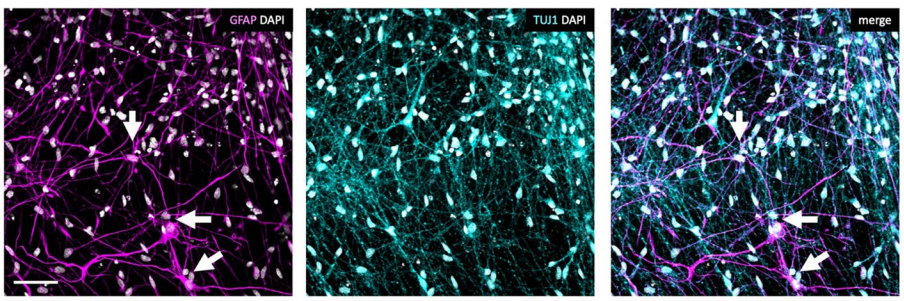

f

#	Maps	-log(pValue)	pValue	FDR
1	Immune response_Oncostatin M signaling via JAK-Stat		5.223e-10	5.208e-7
2	Protein folding and maturation_Posttranslational processing of neuroendocrine peptides		2.391e-9	1.192e-6
3	Oxidative stress_Role of Sirtuin1 and PGC1-alpha in activation of antioxidant defense system		1.545e-8	5.133e-6
4	Gamma-secretase proteolytic targets		2.594e-6	6.465e-4
5	Development_Role of IL-8 in angiogenesis		4.627e-5	9.226e-3
6	TGF-beta signaling via SMADs in breast cancer		6.215e-5	1.033e-2
7	Stellate cells activation and liver fibrosis		7.487e-5	1.066e-2
8	The role of KEAP1/NRF2 pathway in skin sensitization		9.698e-5	1.209e-2
9	Role of metalloproteases and heparanase in progression of pancreatic cancer		1.129e-4	1.244e-2
10	DNA damage_Intra S-phase checkpoint		1.267e-4	1.244e-2

g

GO term ID	GO term description	Strength	FDR
GO:0099061	Integral component of postsynaptic density membrane	0.88	0.0207
GO:0098839	Postsynaptic density membrane	0.72	0.0207
GO:0005912	Adherens junction	0.63	0.013
GO:0045211	Postsynaptic membrane	0.55	0.0101
GO:0097060	Synaptic membrane	0.51	0.0054
GO:0014069	Postsynaptic density	0.51	0.0095
GO:0098984	Neuron to neuron synapse	0.5	0.0094
GO:0098794	Post synapse	0.44	0.0018

Strength = degree of enrichment log10(observed/expected); FDR p-value calculated using Benjamini–Hochberg method

◂**Fig. 5** Challenge of human iPSC neurons with Alzheimer's brain homogenate. (**a**) Immunocytochemistry for dendrites (MAP2, grey), TMEM97 (cyan), post synapses (homer, yellow), and Aβ (6E10, magenta) reveals that Aβ accumulates in TMEM97-containing post synapses in iPSC-derived human neurons challenged with Alzheimer's brain homogenate when the homogenate was mock immunodepleted (Ab+), but not when it was immunodepleted for Aβ (Ab−). DAPI positive cell counts (**b**) and a TUNEL cytotoxicity assay (**c**) show that brain homogenate treatments do not induce cell death. RNA sequencing reveals seven significantly differentially expressed genes between Ab+and Ab− homogenate treatment (**d,** differentially expressed genes with adjusted p value < 0.05 shown in pink in volcano plot). When comparing Aβ challenged cultures treated with CT1812 and vehicle, eight genes are differentially expressed (volcano plot in **e** differentially expressed genes with adjusted p value < 0.05 shown in pink). Staining for astrocytes (GFAP, magenta), neurons (TUJ1, cyan) and nuclei (DAPI, white) reveals that a small proportion of cells in our cultures are astrocytes (arrows) which extend many processes (**f**). Pathway analysis using MetaCore (unadjusted p value < 0.05) shows enrichment of immune/inflammatory pathways with Aβ treatment compared to immunodepleted Aβ treatment (**g**). Using STRING protein interaction analysis of Aβ + Drug vs. Aβ + Vehicle conditions (unadjusted p value < 0.05), the top GO Components (sorted by strength) were involved in synaptic biology (top 8 shown, **h**). Scale bar in panel **a** 20 µm, insets 10 × 10 µm, Scale bar in panel **e** 50 µm

not previously been possible within human synapses. There will be synaptic protein in cell bodies of neurons where they are produced before transport to synapses; however, with our technique, we do not observe somatic labelling of PSD95, rather we observe discrete puncta that are opposed to presynaptic terminal labelling [12].

Here we observe that in human synapses, TMEM97 and Aβ are close enough to generate a FRET effect, an observation that allows us to define close proximity, but does not conclusively show a direct interaction. The fact that we also found a FRET effect between Aβ and PrP_c in the same cases is in line with previous observations [37, 62], and reinforces the idea of multiple synaptic binding partners of Aβ at the synapses of Alzheimer's cases. This is important for the field as both modulating TMEM97 with CT1812 and modulating PrPc rescue cognition in plaque-bearing transgenic mice [15, 27], and these data indicate their beneficial effects could be through a similar mechanism. Given that TMEM97 and PrPc and PrPc and Aβ interact, and given that PrPc has been well characterized to bind Aβ, while it is possible that the interaction with TMEM97 and Aβ is direct, it is also possible that the FRET signal between TMEM97 and Aβ is through a direct interaction of TMEM97 with PrPc, thereby enabling a FRET signal with TMEM97 and Aβ, which is bound to PrPc. With the current methodology, we cannot conclusively determine the proportion of Aβ bound to each potential receptor in synapses but our data do support the idea of protein complexes interacting with Aβ. It is possible that some of the binding partners we observe are acting intracellularly with Aβ after internalization into post synapses.

How this interaction may be leading to synaptic dysfunction and subsequent neurodegeneration is less clear. Several mechanisms have been proposed linking Aβ and synaptic dysfunction involving excitatory imbalance [10, 38]. The fact that we found increased levels of TMEM97 in human Alzheimer's cases and a close proximity between TMEM97 and Aβ at the synapses led us hypothesise that TMEM97 may be involved in the pathogenesis of Alzheimer's and synaptic dysfunction. In the Alzheimer's mouse model included in this study we were able to see a reduction of the Aβ potential binding to TMEM97—as reflected by the decrease of FRET signal—associated with increased estimated receptor occupancy of the investigational drug CT1812, only when using the 80% receptor occupancy threshold for which has been previously reported to be required for efficacy.

Given that variable levels of CT1812, both under and over the 80% RO threshold, were observed in this study, it is not surprising that there was no statistically significant change in mean densities of Aβ, TMEM97 or PSD95 or the synaptic localization of Aβ and/or TMEM97 in the CT1812 treated group compared to vehicle. Post-hoc analyses however focusing on changes that might be mediated in animals for which > 80% RO was achieved was in support of efficacy studies which found this threshold must be achieved for efficacy to be observed: that the increase of estimated receptor occupancy by the drug significantly correlated with a decrease of synaptic FRET signal between Aβ and TMEM97 (rho = − 0.94, $p = 0.017$, Fig. 4F).

The inverse correlation of increasing CT1812 levels with decreased interaction between Aβ and TMEM97 is consistent with the mechanism of action ascribed preclinically, showing a reduction in oligomeric Aβ binding to neuronal synapses in the presence of Sigma-2 receptor modulators [27], and is supportive that CT1812 dosed orally can engage the target, the TMEM97 (Sigma-2) receptor, in the brain, in a drug exposure-dependent manner.

Notably, only five treated mice exhibited drug concentrations above the 80% estimated receptor occupancy, the drug concentration threshold previously defined as effective [27]. The low number of mice with high levels of drug make us cautious about the correlation found while highlight an unexpected finding: a statistically significant increase in drug concentration in male when compared with female mice. None of the variables controlled in the present study could explain the drug concentration differences between males and females and therefore we hypothesise that sex-related biological differences in mouse may be underlying the drug metabolism or blood brain barrier penetration. This is the first study in which CT1812 has been administered to animal models in food, however human clinical trials suggest no difference in CT1812 pharmacokinetics in a fed or fasted state [21]. It is important to note that Izzo and colleagues found an improvement of cognition in mice exhibiting more

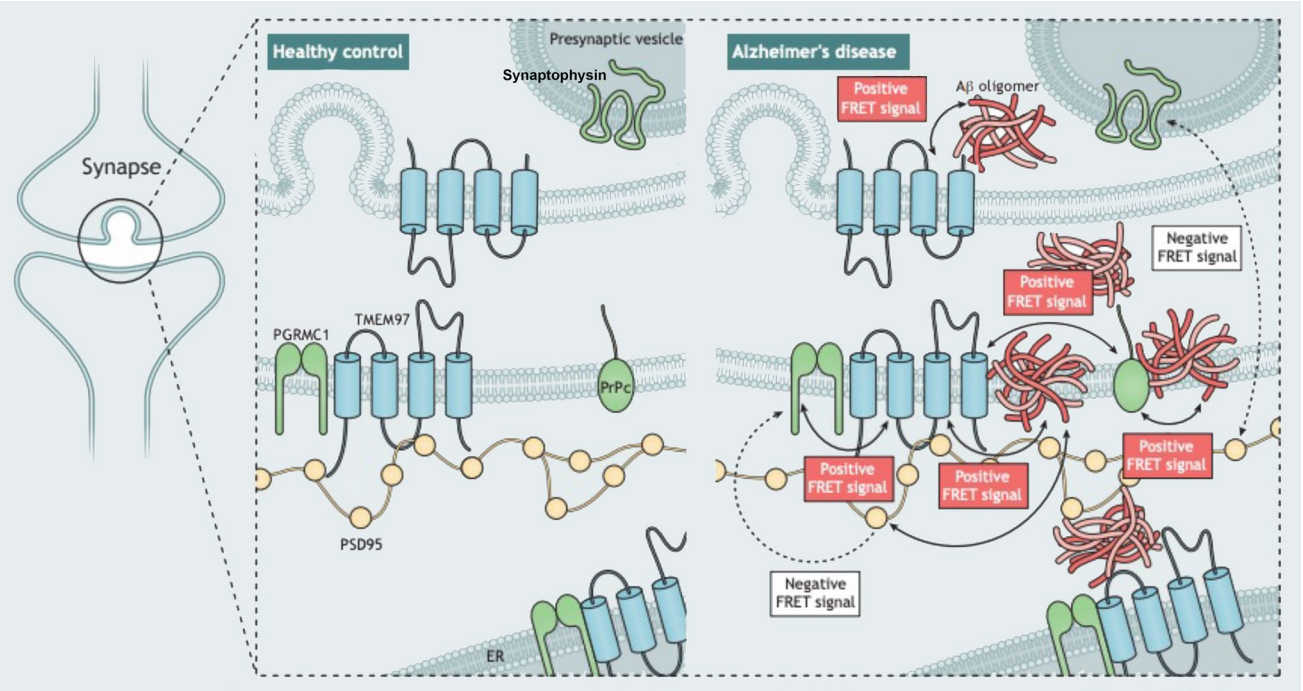

Fig. 6 Model of post-synaptic interactions of Aβ. Based on our study, we observe that Aβ is in close proximity to TMEM97, PSD95, and PrPc. Also, TMEM97-PGRMC1 and TMEM97-PrPc were found close enough to generate FRET signals. There was no FRET signal generated between PGRMC1 and PSD95 nor between PSD95 and synaptophysin which should not be in close enough proximity to generate a signal. These data are consistent with Aβ being a binding partner of these synaptic proteins either at the synaptic membrane or potentially within the post-synapse at spine apparatus

than 80% estimated receptor occupancy, something only seen in one female of our study [27]. Further, Izzo and colleagues included only male mice in the study, and therefore the present findings on female mice should be taken into consideration to ensure the efficacy of treatments in future studies. These findings may be in line with the increasing body of literature describing sex differences in mice models of Alzheimer's that may or may not be translated to human cases [1, 2, 16].

Although we could see a reduction in the synaptic FRET signal of Aβ with TMEM97 in the > 80% estimated receptor occupancy group, and a significant correlation with drug brain concentration in the treated group, the treatment of the Alzheimer's mouse model with TMEM97 modulators did not result in a recovery of synaptic densities nor a decrease of Aβ synaptic localization. CT1812 has been previously demonstrated to selectively displace Aβ oligomers, but not monomer, from synaptic receptor sites and facilitate its clearance out of the brain [27], suggesting that the Aβ that is interacting with TMEM97 observed in this study may be predominantly fibril as opposed to oligomeric. However, disrupting this interaction between TMEM97 and Aβ may be sufficient to improve synaptic function, without requiring a detectable change in synapse density, which could explain the behavioural recovery seen in previous mouse studies with CT1812 treatment [27]. Alternatively, the 28 day treatment period used here may not have been sufficiently long to observe a change in synaptic density; previous studies demonstrating CT1812-mediated improvement in cognitive performance were conducted following 9–10 weeks of administration [27]. Lastly, whereas data herein were generated in the APP/PS1 + Tau mouse model, behavioural data was generated in the Swedish London APP model and it's possible the forms of Aβ most abundant or relative ratios of oligomeric and fibril forms of Aβ are different across Alzheimer's models [27].

A previously published model of CT1812's mechanism of action proposes that the Sigma-2 receptor complex regulates other Aβ oligomer receptors (composed of LilRB2, NGR and PrPc), and when CT1812 binds to TMEM97, allosteric interactions between the Sigma-2 receptor and the oligomer receptor change the oligomer receptors' shape, destabilize the binding pocket, and increase the off-rate of Aβ oligomers from their receptor. Therefore suggesting that CT1812 does not compete directly with oligomers at the same site [28]. In tumor cells, the canonical Sigma-2 ligand DTG binds to Sigma-2 receptors at a location on the TMEM97 protein [3], and CT1812 displaces radiolabeled DTG binding, but the precise binding location of CT1812 has not been directly determined. Our

data indicate that TMEM97 and Aβ are in close proximity where they could be binding, but we cannot rule out that Aβ may be binding to other nearby proteins instead of directly interacting with TMEM97.

In conjunction with FRET showing a synaptic localization, transcriptomic and functional data from human iPSC-derived neuronal cultures treated with soluble fraction of Alzheimer's brain homogenate with the Sigma-2 modulator CT1812 support a synaptic localization and mechanism. UniProt pathway analysis identified "Synapse" as the most significant term in transcripts altered by CT1812 and the top gene ontology terms important are synaptic and include post-synaptic density and post-synaptic membrane. Of the eight transcripts regulated by CT1812 using a highly stringent statistically criterion (B-H adjusted $p < 0.05$) was Protocadherin gamma-B4 (PCDHGB4), a cell adhesion molecule on neuronal synapses, which is involved in synaptic maturation and stabilization [36]. Other amongst the eight top-most significant transcripts altered suggest a role for CT1812 in modulating glia. In the cultures studied, ~ 16% of cells were GFAP + astrocytes and data therefore represents a context of cortical neuron and astrocyte interaction. One of the transcripts significantly changed by CT1812 treatment, CHI3L1, which encodes YKL-40 protein, is expressed in astrocytes and is a biomarker of inflammation in Alzheimer's disease [48]. Beyond the transcript level view, pathway analysis using MetaCore (unadjusted p value < 0.05) revealed enrichment of astrocytic and immune/inflammatory pathways with Aβ treatment compared to immunodepleted Aβ treatment, including the JAK/STAT pathway known to be involved in astrocyte differentiation and function, indicated by LIF and LIFR enrichment, a known pro-inflammatory cytokine involved in the differentiation of neuronal precursor cells into astrocytes (Fig. 5F). We also see in mice that treatment with CT1812 reduces astrogliosis in hippocampus, further supporting an important role for astrocytes in protecting synapses and ultimately cognition. Together, data suggest a role for CT1812 in modulating inflammatory pathways, perhaps indirectly by glia that may detect changes in synapse health or activity. It is possible that some of the TMEM97- Aβ interaction we observed in post synapses contributed to synapse degeneration by glial engulfment as we have recently observed in both human post-mortem tissue and human cellular model systems [70]. In line with the hypothesis of Aβ binding to lipid membranes [38], TMEM97 is thought to be an endo-lysosome-related protein which has itself been linked to cellular toxicity and is essential for the internalization of cholesterol molecules like LDL through the formation of a complex with PGRMC1 [4, 55]. Our transcriptomic data from human iPSC-derived neurons challenged with Alzheimer's brain derived Aβ confirms neuroinflammatory and neurodegenerative related changes with Aβ challenge. Interestingly, in our plaque-bearing mice, CT1812 treatment reduced astrocyte burden in hippocampus, indicating a potential effect of the drug on glial responses.

CT1812 treatment of human iPSC-derived neurons caused multiple changes in transcripts involved in synaptic function, consistent with the ability of CT1812 to influence synapses and potentially ameliorate damage in Alzheimer's. Our functional data using calcium imaging similarly showed an interaction between CT1812 and Aβ treatment, however, these results should be interpreted with caution as the cells after 24 h of pre-incubation with human brain homogenate did not appear as healthy as the cells which had acute treatment, and we only had capacity to image 1–2 cell lines per group (albeit with hundreds of imaged objects) in the 24 h condition. However, these data do conclusively demonstrate that our iPSC-derived neurons are active at 180 days post-differentiation—the time point when RNA was also collected for sequencing—and that acutely across lines from 3 donors that CT1812 treatment does not cause excessive excitation.

In summary, in human Alzheimer's brains we found increased synaptic levels of TMEM97 and close colocalization of TMEM97 with Aβ in synapses. This supports the idea that TMEM97 is a synaptic binding partner for Aβ either directly or indirectly, which is important as this interaction can be modulated by drugs.

Acknowledgements The authors thank our brain tissue donors and their families for their generous donations. Authors gratefully acknowledge membership of Edinburgh Neuroscience. Some of the control participants in the human study were from the Lothian Birth Cohort 1936, thus we wish to thank the cohort and research team supported by Age UK (Disconnected Mind project) in The University of Edinburgh Centre for Cognitive Ageing and Cognitive Epidemiology, funded by the Biotechnology and Biological Sciences Research Council (BBSRC) and Medical Research Council (MRC) ((MR/K026992/1). We also acknowledge Neil Smith for artwork in Figure 6.

Funding This work was supported by Alzheimer's Society (project grant AS-PG-15b-023), Alzheimer's Research UK, the European Research Council (ERC) under the European Union's Horizon 2020 research and innovation programme (Grant agreement No. 681181), the University of Edinburgh (Chancellor's Fellow start-up funding), Wellcome Trust Institutional Strategic Support Fund, the UK Dementia Research Institute which receives its funding from DRI Ltd., funded by the UK Medical Research Council, Alzheimer's Society, and Alzheimer's Research UK (UKDRI-Edin005), and BBSRC Institute Strategic Programme funding.

Data availability Protocols, image analysis scripts and R scripts for statistical analysis are available at https://doi.org/10.7488/ds/7664. Raw images available from the corresponding author upon reasonable request.

Declarations

Conflict of interest TSJ is a member of the Scientific Advisory Board of Cognition Therapeutics and Scottish Brain Sciences. NI, LW, and SC were employees of Cognition Therapeutics, and MEH and AOC are current employees of Cognition Therapeutics.

References

1. Abd-Elrahman KS, Albaker A, de Souza JM, Ribeiro FM, Schlossmacher MG, Tiberi M et al (2020) Aβ oligomers induce pathophysiological mGluR5 signaling in Alzheimer's disease model mice in a sex-selective manner. Sci Signal. https://doi.org/10.1126/scisignal.abd2494
2. Agostini A, Yuchun D, Li B, Kendall DA, Pardon M-C (2020) Sex-specific hippocampal metabolic signatures at the onset of systemic inflammation with lipopolysaccharide in the APPswe/PS1dE9 mouse model of Alzheimer's disease. Brain Behav Immun 83:87–111. https://doi.org/10.1016/j.bbi.2019.09.019
3. Alon A, Schmidt HR, Wood MD, Sahn JJ, Martin SF, Kruse AC (2017) Identification of the gene that codes for the σ2 receptor. Proc Natl Acad Sci USA 114:7160–7165. https://doi.org/10.1073/pnas.1705154114
4. Bartz F, Kern L, Erz D, Zhu M, Gilbert D, Meinhof T et al (2009) Identification of cholesterol-regulating genes by targeted RNAi screening. Cell Metab 10:63–75. https://doi.org/10.1016/j.cmet.2009.05.009
5. Benilova I, De Strooper B (2013) Promiscuous Alzheimer's amyloid: yet another partner. Science 341:1354–1355. https://doi.org/10.1126/science.1244166
6. Bilousova T, Miller CA, Poon WW, Vinters HV, Corrada M, Kawas C et al (2016) Synaptic amyloid-β oligomers precede p-tau and differentiate high pathology control cases. Am J Pathol 186:185–198. https://doi.org/10.1016/j.ajpath.2015.09.018
7. Braak H, Alafuzoff I, Arzberger T, Kretzschmar H, Del Tredici K (2006) Staging of Alzheimer disease-associated neurofibrillary pathology using paraffin sections and immunocytochemistry. Acta Neuropathol 112:389–404. https://doi.org/10.1007/s00401-006-0127-z
8. Cassano G, Gasparre G, Niso M, Contino M, Scalera V, Colabufo NA (2009) F281, synthetic agonist of the sigma-2 receptor, induces Ca2+ efflux from the endoplasmic reticulum and mitochondria in SK-N-SH cells. Cell Calcium 45:340–345. https://doi.org/10.1016/j.ceca.2008.12.005
9. Cavanaugh JE, Neath AA (2019) The Akaike information criterion: background, derivation, properties, application, interpretation, and refinements. WIREs Comput Stat 11:e1460. https://doi.org/10.1002/wics.1460
10. Chen Y, Fu AKY, Ip NY (2019) Synaptic dysfunction in Alzheimer's disease: mechanisms and therapeutic strategies. Pharmacol Ther 195:186–198. https://doi.org/10.1016/j.pharmthera.2018.11.006
11. Cognition Therapeutics (2020) A Randomized, double-blind, placebo-controlled, parallel-group, phase 2 study to evaluate the safety and efficacy of CT1812 in subjects with mild to moderate Alzheimer's disease. https://iadrp.nia.nih.gov/project/randomized-double-blind-placebo-controlled-parallel-group-phase-ii-study-evaluate-safety-1
12. Colom-Cadena M, Davies C, Sirisi S, Lee J-E, Simzer EM, Tzioras M et al (2023) Synaptic oligomeric tau in Alzheimer's disease—a potential culprit in the spread of tau pathology through the brain. Neuron 111:2170-2183.e6. https://doi.org/10.1016/j.neuron.2023.04.020
13. Colom-Cadena M, Pegueroles J, Herrmann AG, Henstridge CM, Muñoz L, Querol-Vilaseca M et al (2017) Synaptic phosphorylated α-synuclein in dementia with Lewy bodies. Brain 140:3204–3214. https://doi.org/10.1093/brain/awx275
14. Colom-Cadena M, Spires-Jones T, Zetterberg H, Blennow K, Caggiano A, DeKosky ST et al (2020) The clinical promise of biomarkers of synapse damage or loss in Alzheimer's disease. Alzheimers Res Ther. https://doi.org/10.1186/s13195-020-00588-4
15. Cox TO, Gunther EC, Brody AH, Chiasseu MT, Stoner A, Smith LM et al (2019) Anti-PrPC antibody rescues cognition and synapses in transgenic alzheimer mice. Ann Clin Transl Neurol 6:554–574. https://doi.org/10.1002/acn3.730
16. Davis EJ, Broestl L, Abdulai-Saiku S, Worden K, Bonham LW, Miñones-Moyano E et al (2020) A second X chromosome contributes to resilience in a mouse model of Alzheimer's disease. Sci Transl Med. https://doi.org/10.1126/scitranslmed.aaz5677
17. DeKosky ST, Scheff SW (1990) Synapse loss in frontal cortex biopsies in Alzheimer's disease: correlation with cognitive severity. Ann Neurol 27:457–464. https://doi.org/10.1002/ana.410270502
18. Dobin A, Davis CA, Schlesinger F, Drenkow J, Zaleski C, Jha S et al (2013) STAR: ultrafast universal RNA-seq aligner. Bioinformatics 29:15–21. https://doi.org/10.1093/bioinformatics/bts635
19. Forner S, Baglietto-Vargas D, Martini AC, Trujillo-Estrada L, LaFerla FM (2017) Synaptic impairment in Alzheimer's disease: a dysregulated symphony. Trends Neurosci 40:347–357. https://doi.org/10.1016/j.tins.2017.04.002
20. Förster T (1967) Chapter II - Mechanisms of Energy Transfer. In: Comprehensive Biochemistry, vol 22, pp 61–80. https://doi.org/10.1016/B978-1-4831-9712-8.50010-2
21. Grundman M, Morgan R, Lickliter JD, Schneider LS, DeKosky S, Izzo NJ et al (2019) A phase 1 clinical trial of the sigma-2 receptor complex allosteric antagonist CT1812, a novel therapeutic candidate for Alzheimer's disease. Alzheimers Dement (N Y) 5:20–26. https://doi.org/10.1016/j.trci.2018.11.001
22. Guo L, Zhen X (2015) Sigma-2 receptor ligands: neurobiological effects. Curr Med Chem 22:989–1003. https://doi.org/10.2174/0929867322666150114163607
23. Hellenkamp B, Schmid S, Doroshenko O, Opanasyuk O, Kühnemuth R, Rezaei Adariani S et al (2018) Precision and accuracy of single-molecule FRET measurements-a multi-laboratory benchmark study. Nat Methods 15:669–676. https://doi.org/10.1038/s41592-018-0085-0
24. Henstridge CM, Hyman BT, Spires-Jones TL (2019) Beyond the neuron–cellular interactions early in Alzheimer disease pathogenesis. Nat Rev Neurosci 20:94–108. https://doi.org/10.1038/s41583-018-0113-1
25. Hesse R, Hurtado ML, Jackson RJ, Eaton SL, Herrmann AG, Colom-Cadena M et al (2019) Comparative profiling of the synaptic proteome from Alzheimer's disease patients with focus on the APOE genotype. Acta Neuropathol Commun 7:214. https://doi.org/10.1186/s40478-019-0847-7
26. Hong W, Wang Z, Liu W, O'Malley TT, Jin M, Willem M et al (2018) Diffusible, highly bioactive oligomers represent a critical minority of soluble Aβ in Alzheimer's disease brain. Acta Neuropathol 136:19–40. https://doi.org/10.1007/s00401-018-1846-7
27. Izzo NJ, Staniszewski A, To L, Fa M, Teich AF, Saeed F et al (2014) Alzheimer's therapeutics targeting amyloid beta 1–42

oligomers I: Abeta 42 oligomer binding to specific neuronal receptors is displaced by drug candidates that improve cognitive deficits. PLoS ONE 9:e111898. https://doi.org/10.1371/journal.pone.0111898
28. Izzo NJ, Yuede CM, LaBarbera KM, Limegrover CS, Rehak C, Yurko R et al (2021) Preclinical and clinical biomarker studies of CT1812: A novel approach to Alzheimer's disease modification. Alzheimers Dement 17:1365–1382. https://doi.org/10.1002/alz.12302
29. Jackson RJ, Rose J, Tulloch J, Henstridge C, Smith C, Spires-Jones TL (2019) Clusterin accumulates in synapses in Alzheimer's disease and is increased in apolipoprotein E4 carriers. Brain Commun 1:fcz003. https://doi.org/10.1093/braincomms/fcz003
30. Jarosz-Griffiths HH, Noble E, Rushworth JV, Hooper NM (2016) Amyloid-β receptors: the good, the bad, and the prion protein. J Biol Chem 291:3174–3183. https://doi.org/10.1074/jbc.R115.702704
31. Kay KR, Smith C, Wright AK, Serrano-Pozo A, Pooler AM, Koffie R et al (2013) Studying synapses in human brain with array tomography and electron microscopy. Nat Protoc 8:1366–1380. https://doi.org/10.1038/nprot.2013.078
32. Kim T, Vidal GS, Djurisic M, William CM, Birnbaum ME, Garcia KC et al (2013) Human LilrB2 Is a β-amyloid receptor and its murine homolog pirB regulates synaptic plasticity in an Alzheimer's model. Science 341:1399–1404. https://doi.org/10.1126/science.1242077
33. King D, Holt K, Toombs J, He X, Dando O, Okely JA et al (2022) Synaptic resilience is associated with maintained cognition during ageing. Alzheimers Dement 19:2560–2574
34. Koffie RM, Hashimoto T, Tai H-C, Kay KR, Serrano-Pozo A, Joyner D et al (2012) Apolipoprotein E4 effects in Alzheimer's disease are mediated by synaptotoxic oligomeric amyloid-β. Brain 135:2155–2168. https://doi.org/10.1093/brain/aws127
35. Lacor PN, Buniel MC, Chang L, Fernandez SJ, Gong Y, Viola KL et al (2004) Synaptic targeting by Alzheimer's-related amyloid beta oligomers. J Neurosci 24:10191–10200. https://doi.org/10.1523/JNEUROSCI.3432-04.2004
36. LaMassa N, Sverdlov H, Mambetalieva A, Shapiro S, Bucaro M, Fernandez-Monreal M et al (2021) Gamma-protocadherin localization at the synapse is associated with parameters of synaptic maturation. J Comp Neurol 529:2407–2417. https://doi.org/10.1002/cne.25102
37. Laurén J, Gimbel DA, Nygaard HB, Gilbert JW, Strittmatter SM (2009) Cellular prion protein mediates impairment of synaptic plasticity by amyloid-β oligomers. Nature 457:1128–1132. https://doi.org/10.1038/nature07761
38. Li S, Selkoe DJ (2020) A mechanistic hypothesis for the impairment of synaptic plasticity by soluble Aβ oligomers from Alzheimer's brain. J Neurochem 154:583–597. https://doi.org/10.1111/jnc.15007
39. Liao Y, Smyth GK, Shi W (2014) featureCounts: an efficient general purpose program for assigning sequence reads to genomic features. Bioinformatics 30:923–930. https://doi.org/10.1093/bioinformatics/btt656
40. Love MI, Huber W, Anders S (2014) Moderated estimation of fold change and dispersion for RNA-seq data with DESeq2. Genome Biol 15:550. https://doi.org/10.1186/s13059-014-0550-8
41. Lue LF, Kuo YM, Roher AE, Brachova L, Shen Y, Sue L et al (1999) Soluble amyloid beta peptide concentration as a predictor of synaptic change in Alzheimer's disease. Am J Pathol 155:853–862. https://doi.org/10.1016/s0002-9440(10)65184-x
42. Martinkova J, Quevenco F-C, Karcher H, Ferrari A, Sandset EC, Szoeke C et al (2021) Proportion of women and reporting of outcomes by sex in clinical trials for Alzheimer disease: a systematic review and meta-analysis. JAMA Netw Open 4:e2124124. https://doi.org/10.1001/jamanetworkopen.2021.24124
43. Micheva KD, Smith SJ (2007) Array tomography: a new tool for imaging the molecular architecture and ultrastructure of neural circuits. Neuron 55:25–36. https://doi.org/10.1016/j.neuron.2007.06.014
44. Mondal S, Hegarty E, Sahn JJ, Scott LL, Gökçe SK, Martin C et al (2018) High-content microfluidic screening platform used to identify σ2R/Tmem97 binding ligands that reduce age-dependent neurodegeneration in C. elegans SC_APP model. ACS Chem Neurosci 9:1014–1026. https://doi.org/10.1021/acschemneuro.7b00428
45. Montine TJ, Phelps CH, Beach TG, Bigio EH, Cairns NJ, Dickson DW et al (2012) National Institute on Aging-Alzheimer's Association guidelines for the neuropathologic assessment of Alzheimer's disease: a practical approach. Acta Neuropathol 123:1–11. https://doi.org/10.1007/s00401-011-0910-3
46. Mroczko B, Groblewska M, Litman-Zawadzka A, Kornhuber J, Lewczuk P (2018) Cellular receptors of amyloid β oligomers (AβOs) in Alzheimer's disease. Int J Mol Sci 19:1884. https://doi.org/10.3390/ijms19071884
47. Murphy M, Pykett MJ, Harnish P, Zang KD, George DL (1993) Identification and characterization of genes differentially expressed in meningiomas. Cell Growth Differ 4:715–722
48. Olsson B, Lautner R, Andreasson U, Öhrfelt A, Portelius E, Bjerke M et al (2016) CSF and blood biomarkers for the diagnosis of Alzheimer's disease: a systematic review and meta-analysis. Lancet Neurol 15:673–684. https://doi.org/10.1016/S1474-4422(16)00070-3
49. Parri HR, Hernandez CM, Dineley KT (2011) Research update: Alpha7 nicotinic acetylcholine receptor mechanisms in Alzheimer's disease. Biochem Pharmacol 82:931–942. https://doi.org/10.1016/j.bcp.2011.06.039
50. Pham E, Crews L, Ubhi K, Hansen L, Adame A, Cartier A et al (2010) Progressive accumulation of amyloid-beta oligomers in Alzheimer's disease and in amyloid precursor protein transgenic mice is accompanied by selective alterations in synaptic scaffold proteins. FEBS J 277:3051–3067. https://doi.org/10.1111/j.1742-4658.2010.07719.x
51. Pickett EK, Herrmann AG, McQueen J, Abt K, Dando O, Tulloch J et al (2019) Amyloid beta and tau cooperate to cause reversible behavioral and transcriptional deficits in a model of Alzheimer's disease. Cell Rep 29:3592–3604.e5. https://doi.org/10.1016/j.celrep.2019.11.044
52. Pickett EK, Koffie RM, Wegmann S, Henstridge CM, Herrmann AG, Colom-Cadena M et al (2016) Non-fibrillar oligomeric amyloid-β within synapses. J Alzheimers Dis 53:787–800. https://doi.org/10.3233/JAD-160007
53. R Core Team (2017) R: a language and environment for statistical computing. https://www.R-project.org/. Accessed 12 Sep 2020
54. Riad A, Lengyel-Zhand Z, Zeng C, Weng C-C, Lee VM-Y, Trojanowski JQ et al (2020) The sigma-2 receptor/TMEM97, PGRMC1, and LDL receptor complex are responsible for the cellular uptake of Aβ42 and its protein aggregates. Mol Neurobiol 57:3803–3813. https://doi.org/10.1007/s12035-020-01988-1
55. Riad A, Zeng C, Weng C-C, Winters H, Xu K, Makvandi M et al (2018) Sigma-2 receptor/TMEM97 and PGRMC-1 increase the rate of internalization of LDL by LDL receptor through the formation of a ternary complex. Sci Rep 8:16845. https://doi.org/10.1038/s41598-018-35430-3
56. Scheff SW, Price DA, Schmitt FA, Mufson EJ (2006) Hippocampal synaptic loss in early Alzheimer's disease and mild cognitive impairment. Neurobiol Aging 27:1372–1384. https://doi.org/10.1016/j.neurobiolaging.2005.09.012
57. Schindelin J, Arganda-Carreras I, Frise E, Kaynig V, Longair M, Pietzsch T et al (2012) Fiji: an open-source platform for

biological-image analysis. Nat Methods 9:676–682. https://doi.org/10.1038/nmeth.2019
58. Schmidt HR, Kruse AC (2019) The molecular function of σ receptors: past, present, and future. Trends Pharmacol Sci 40:636–654. https://doi.org/10.1016/j.tips.2019.07.006
59. Schneider CA, Rasband WS, Eliceiri KW (2012) NIH image to imageJ: 25 years of image analysis. Nat Methods 9:671–675. https://doi.org/10.1038/nmeth.2089
60. Shankar GM, Li S, Mehta TH, Garcia-Munoz A, Shepardson NE, Smith I et al (2008) Amyloid-beta protein dimers isolated directly from Alzheimer's brains impair synaptic plasticity and memory. Nat Med 14:837–842. https://doi.org/10.1038/nm1782
61. Shi Y, Kirwan P, Livesey FJ (2012) Directed differentiation of human pluripotent stem cells to cerebral cortex neurons and neural networks. Nat Protoc 7:1836–1846. https://doi.org/10.1038/nprot.2012.116
62. Smith LM, Kostylev MA, Lee S, Strittmatter SM (2019) Systematic and standardized comparison of reported amyloid-β receptors for sufficiency, affinity, and Alzheimer's disease relevance. J Biol Chem 294:6042–6053. https://doi.org/10.1074/jbc.RA118.006252
63. Smith LM, Strittmatter SM (2017) Binding sites for amyloid-β oligomers and synaptic toxicity. Cold Spring Harb Perspect Med 7:a024075. https://doi.org/10.1101/cshperspect.a024075
64. Spires-Jones TL, Hyman BT (2014) The intersection of amyloid beta and tau at synapses in Alzheimer's disease. Neuron 82:756–771. https://doi.org/10.1016/j.neuron.2014.05.004
65. Takahashi RH, Almeida CG, Kearney PF, Yu F, Lin MT, Milner TA et al (2004) Oligomerization of Alzheimer's β-amyloid within processes and synapses of cultured neurons and brain. J Neurosci 24:3592–3599. https://doi.org/10.1523/JNEUROSCI.5167-03.2004
66. Takahashi RH, Milner TA, Li F, Nam EE, Edgar MA, Yamaguchi H et al (2002) Intraneuronal Alzheimer abeta42 accumulates in multivesicular bodies and is associated with synaptic pathology. Am J Pathol 161:1869–1879. https://doi.org/10.1016/s0002-9440(10)64463-x
67. Terry RD, Masliah E, Salmon DP, Butters N, DeTeresa R, Hill R et al (1991) Physical basis of cognitive alterations in alzheimer's disease: synapse loss is the major correlate of cognitive impairment. Ann Neurol 30:572–580. https://doi.org/10.1002/ana.410300410
68. Thal DR, Rüb U, Orantes M, Braak H (2002) Phases of A beta-deposition in the human brain and its relevance for the development of AD. Neurology 58:1791–1800. https://doi.org/10.1212/wnl.58.12.1791
69. Toombs J, Panther L, Ornelas L, Liu C, Gomez E, Martín-Ibáñez R et al (2020) Generation of twenty four induced pluripotent stem cell lines from twenty four members of the lothian birth cohort 1936. Stem Cell Res 46:101851. https://doi.org/10.1016/j.scr.2020.101851
70. Tzioras M, Daniels MJD, Davies C, Baxter P, King D, McKay S et al (2023) Human astrocytes and microglia show augmented ingestion of synapses in Alzheimer's disease via MFG-E8. Cell Rep Med. https://doi.org/10.1016/j.xcrm.2023.101175
71. Tzioras M, McGeachan RI, Durrant CS, Spires-Jones TL (2023) Synaptic degeneration in Alzheimer disease. Nat Rev Neurol 19:19–38. https://doi.org/10.1038/s41582-022-00749-z
72. Um JW, Kaufman AC, Kostylev M, Heiss JK, Stagi M, Takahashi H et al (2013) Metabotropic glutamate receptor 5 is a coreceptor for Alzheimer aβ oligomer bound to cellular prion protein. Neuron 79:887–902. https://doi.org/10.1016/j.neuron.2013.06.036
73. Vargas LM, Leal N, Estrada LD, González A, Serrano F, Araya K et al (2014) EphA4 activation of c-Abl mediates synaptic loss and LTP blockade caused by amyloid-β oligomers. PLoS ONE 9:e92309. https://doi.org/10.1371/journal.pone.0092309
74. Vilner BJ, Bowen WD (2000) Modulation of cellular calcium by sigma-2 receptors: release from intracellular stores in human SK-N-SH neuroblastoma cells. J Pharmacol Exp Ther 292:900–911
75. Wouters FS, Verveer PJ, Bastiaens PI (2001) Imaging biochemistry inside cells. Trends Cell Biol 11:203–211. https://doi.org/10.1016/s0962-8924(01)01982-1
76. Yeap J, Sathyaprakash C, Toombs J, Tulloch J, Scutariu C, Rose J et al (2022) Reducing voltage-dependent potassium channel Kv3.4 levels ameliorates synapse loss in a mouse model of Alzheimer's disease. Brain Neurosci Adv 6:23982128221086464. https://doi.org/10.1177/23982128221086464
77. Yi B, Sahn JJ, Ardestani PM, Evans AK, Scott L, Chan JZ et al (2017) Small molecule modulator of sigma 2 receptor is neuroprotective and reduces cognitive deficits and neuro-inflammation in experimental models of Alzheimer's disease. J Neurochem 140:561–575. https://doi.org/10.1111/jnc.13917
78. Zeng C, Weng C-C, Schneider ME, Puentes L, Riad A, Xu K et al (2019) TMEM97 and PGRMC1 do not mediate sigma-2 ligand-induced cell death. Cell Death Discovery 5:1–12. https://doi.org/10.1038/s41420-019-0141-2
79. Zhang Y, Zhao Y, Zhang L, Yu W, Wang Y, Chang W (2019) Cellular prion protein as a receptor of toxic amyloid-β42 oligomers is important for Alzheimer's disease. Front Cell Neurosci 13:339. https://doi.org/10.3389/fncel.2019.00339
80. Zimmermann T (2019) Photobleaching and sensitized emission-based methods for the detection of förster resonance energy transfer. Methods Mol Biol 2040:235–274. https://doi.org/10.1007/978-1-4939-9686-5_12
81. STRING v11: protein-protein association networks with increased coverage, supporting functional discovery in genome-wide experimental datasets—PubMed. https://pubmed.ncbi.nlm.nih.gov/30476243/. Accessed 15 Nov 2022